

LASER PYROLYSIS OF AN ENTRAINED STREAM OF COAL PARTICLES

Michael W. Smith, Donald F. McMillen,
Ripudaman Malhotra, and Robert M. Platz

Chemical Kinetics Department, Chemistry Laboratory
SRI International, Menlo Park California, 94025-3493

KEYWORDS: Coal Pyrolysis, Laser-heated, PCAH additives.

INTRODUCTION

In the search for efficient ways to convert coals to liquid fuels or other hydrocarbon products, the relative simplicity of pyrolysis has for a long time been recognized as a very attractive feature. However, char yields are typically high and volatile products are generally dominated by light hydrocarbons and tars that can be extremely difficult to upgrade. Efforts to guide research directed toward improved yields in pyrolysis processes have been hampered by the acceptance of a traditional mechanism that is, at best, incomplete (1).

In order to contribute to an improved understanding of the chemical and physical processes that control the formation of volatiles during coal pyrolysis, we have developed an apparatus for pyrolyzing coal particles entrained in cold gas with a CW infrared laser. (2) This approach results in very rapid in-depth heating of the coal to a steady-state temperature, which is determined by the balance between radiative input to the particle and the sum of convective and radiative heat losses to the cold gas. The advantages of this pyrolysis mode are that (i) it provides a very rapid heat-up to a steady state temperature and thus a close approximation to the idealized temperature-jump experiment; (ii) initially produced volatiles are evolved into a cold-gas atmosphere such that secondary reactions obscuring the nature of the original volatiles producing chemistry will tend to be minimized; and (iii) substantial quantities of coal are pyrolyzed making subsequent analysis of the tars and chars possible, something which is not possible with a single-particle approach. The difficulties of the approach involve the necessity to provide very constant flow rates and particle loadings and laser illumination that is constant with time and space in the heated region and is also reasonably omni-directional; the difficulties also involve the inescapable reality that even a narrow physical and aerodynamic particle size distribution will still result in some range of particle velocities, residence times, and steady-state temperatures.

A particular goal of this work is to use entrained-flow laser pyrolysis as one of the tools to explore the benefits that may be achieved by treating coals before pyrolysis with small amounts of high-boiling additives. The rationale for such an approach, along with some preliminary results using conventional heating methods, has been reported previously (3). In brief, in pyrolysis, meeting the stoichiometric and kinetic requirements of bond cleavage is especially crucial: not only is there no solvent to supply hydrogen as there is in liquefaction, but any hydrogen fed to the reaction zone is known (4) to be relatively ineffective at short reaction times and temperatures below $\sim 700^{\circ}\text{C}$. Therefore, it may be possible to achieve substantially increased yields of condensable volatiles, if pre-treatment with partially hydrogenated coal tars can (i) supply a small amount of critically needed hydrogen in a kinetically accessible form, and (ii) increase the efficiency with which the indigenous coal hydrogen can itself be shuttled from hydrogen-rich portions of the coal structure to more hydrogen-poor regions to aid in bond cleavage. Figure 1 summarizes the way by which polycyclic aromatic hydrocarbons (PCAH) tend to increase H-utilization efficiency in light of recently described chemistry (5-7): PCAH can serve to recover hydrogen atoms that have been transferred to positions where no linkage cleavage can occur. This recovery helps to re-direct hydroaromatic hydrogen from light hydrocarbon formation (ring-reduction and cracking) to cleavage of inter-cluster linkages.

LASER PYROLYSIS TECHNIQUE

Particle Flow

Schematic diagram of the laser-pyrolysis apparatus is shown in Figure 2. The coals are ground under nitrogen (or in the case of the Argonne -100 mesh samples, taken directly from the vials), wet-sieved, and dried for 18 hours under vacuum at 65°C. Several grams of the 270/230 mesh fraction (nominal 53 to 63 μm) are loaded into the hopper of a rotating-disc dust-feeder which feeds a fluidized bed, using argon as the entrainment gas. This bed in turn feeds the inlet of the 3-mm id ejector tube, the outlet of which is just downstream of an aluminum honeycomb flow straightener, and 3 to 5 mm upstream of the region where the IR laser beam crosses the axis of particle flow. The length of the illuminated region can be varied from 3 to about 20 mm. Condensable volatiles are either ejected from the pyrolyzing coal particles as an aerosol, or quickly form one when they hit the cold argon stream. Several mm downstream of the heated zone, the tar-aerosol and char particle stream enter a collector with an 8-mm id and a conical interior that smoothly decreases to 3 mm. The flow then passes through a miniature cyclone designed to collect particles larger than ca. 10 μm . The tar aerosol (typically 0.2 to 0.3 μm diameter), and any other small particles, pass through the cyclone and are collected on one of a pair of filters in a parallel-flow filter arrangement.

The char-tar separation is typically very good: microscopic examination shows the cake on the final filter to consist of tawny yellow tar aerosol particles, entirely free of black coal- or char-particles of any size. The cyclone contained all the char, with small amounts of tar aerosol attached to some of the char particles, evidently as the result of collisions within the cyclone. Since the aerosol particles were ca. 0.3 μm , as compared with the ca. 50- μm char particles, the mass fraction of tar contaminating the char was very low; typically less than 5%. This tar contamination could easily be removed from the char by a quick THF wash, either before char analysis, or for purposes of correcting the % yield of tar.

Gas Flow Control

The flow control system leading to and from the laser pyrolysis apparatus consists of four streams: the ejector- and collector- flows, and the ejector- and collector- sheath flows. Because flow through the ejector tube (ca. 50 cc/min) is not controllable directly, but is constrained to be equal to the sum of the collector- and the collector-sheath- flows minus the ejector sheath flow, and the two sheath flow are each about 5 liters/min, small percentage changes in either of the sheath flows would result in a large percentage change in the ejector flow. Therefore, fine positive control of the sheath gas is maintained by routing ca. 97% of their flow through single-stage regulators and over a fixed flow-control orifice. The remaining 3% is shunted through a pair of 0 to 500-cc/min mass flow controllers (Tylan). The flows are adjusted to control the ejector gas flow at the desired volumetric flow, typically set so that the ejector and its sheath flow have nearly equal space velocities.

Laser Beam Manipulation

The beam from a Coherent Model 41 CW CO₂ laser is passed through an 8-mm orifice in a graphite disc to remove the fringes, and is then directed to the cell by two flat and one slightly concave (20-m radius of curvature) copper mirrors. Immediately in front of the pyrolysis cell, the beam is focused through a point using a 1-in focal length zinc selenide lens, and allowed to expand into a channel integrator consisting of polished aluminum plates bolted together to form a channel having a 6.5-mm square opening. The divergent radiation that exits this channel is then imaged with a second lens through the KCl window in the pyrolysis cell and onto the axis of particle flow. The "beam" diverges after passing through the particle stream, and is re-imaged back on the flow axis by a concave copper mirror on the back side of the cell. The radiation that is not absorbed by the second pass diverges as it exits through the KCl window and is absorbed by a graphite beam block.

As shown schematically in Figure 3, the channel integrator converts the Gaussian profile of the laser beam into a profile that, on a microscopic scale, is flat across the entire image. Fresnel diffraction results in a series of peaks and valleys in the intensity, but these are on a microscopic

scale, with the peak-to-peak distance being ca. 200 μm , and are suitably averaged by retro-reflection under conditions where the stream of particles is optically thin.

Pretreatment of Coals and Product Analysis

The additive used in this work was a partially hydrogenated coal tar. The field ionization mass spectrum of the parent tar is shown in Figure 4. The spectrum clearly indicates that the tar is composed almost entirely of polycyclic aromatic hydrocarbons, with the most prominent PCAH structure being pyrene. In the spectrum obtained after hydrogenation (not shown), examination of the various M+2 and M+4 peaks shows that the degree of hydrogenation increases with increasing ring size. For example, ~22% of the pyrene, but 37% of the di-benzopyrenes were converted by the mild hydrogenation to di- or tetra- hydroaromatics. The coals were loaded with 8 to 10% of the hydrogenated tar, using tetrahydrofuran (THF) as the solvent employing the technique of incipient wetness to minimize preferential deposition of the additive at the particle surface and/or THF-extraction of soluble materials from the coal. The THF was removed by drying in a vacuum oven at 65°C for 18 hours. Some pyrolysis experiments were performed with THF-only treated coals to serve as appropriate blanks.

The primary analytical technique used thus far for examination of the tars and the chars has been field ionization mass spectrometry (FIMS). The use of the instrument at SRI has been extensively described in the literature (8); a series of unit-resolution mass spectra are recorded as the sample is heated in a temperature-programmed inlet (typically at 3°C/s, up to 450°C). From these data, the temperature evolution profile of any nominal mass or group of masses can be plotted, including a vacuum evaporation - or micro distillation- curve representing the sum of all volatiles. Although nominal mass provides no direct identification of the molecular formula of the particular molecular ion, in the low molecular weight range (m/z 50-150), and for prominent peaks at certain characteristic masses above that range, inspection can usually provide very reliable identification (8).

RESULTS AND DISCUSSION

The Impact of Pretreatment on Tar Yields

Figure 5 shows the impact of the tar pretreatment under laser-pyrolysis conditions, and for comparison, Figure 6 shows the impact observed under vacuum TGA conditions. (All of the yields were based on the assumption that the tar added in the pretreatment was itself fully volatilized.) Under the laser-pyrolysis conditions used thus far, the pretreated Pittsburgh No. 8 (Argonne) showed a substantial increase in tar yield (20%), but the pretreated Illinois No. 6 and Wyodak coals (Argonne), gave average corrected yields that were actually significantly lower than those for the untreated (but dried) coal. On the other hand, pyrolysis under TGA conditions resulted in 31 and 11% increases in yields of total volatiles for the pretreated Wyodak and Illinois No.6 coals, respectively, as well as an increase of 24% for the pretreated Pittsburgh No. 8 (Clovis Point Mine, and PSOC coals 1098 and 1099, respectively). The pretreated and the blank coals were not exactly identical in the two sets of pyrolysis experiments. However, for the reasons discussed below, we believe that the smaller benefit and less consistent improvement obtained under laser pyrolysis conditions resulted primarily from the fact that the final pyrolysis temperatures in the laser pyrolysis were more than 200°C higher. We therefore project that improving the yield-enhancing impact of the pretreatment entails pushing the laser-pyrolysis conditions further towards lower temperatures and longer times.

Since the amount of hydrogen actually supplied by the hydroaromatics added in the pretreatment is very small, it is important that this hydrogen be used with maximum efficiency, and that the added PCAH operate with maximum effectiveness in promoting the use of indigenous hydrogen. In order to meet these criteria, it is necessary to reach the temperature region of widespread radical reactions (i.e., 400 to 500°C), as these reactions are what bring about the H-atom transfer that results in hydrogenolysis. However, as the temperature increases, the PCAH in the reaction mixture are less and less able to recover hydrogen transferred to positions bearing no linkages (1,7). Optimum temperatures for conversion will thus be a compromise between reactivity and efficiency in hydrogen utilization.

We based our initial choice of conditions for the TGA pyrolyses that might constitute such a compromise on the work of Fong and Howard (9) on the evolution of volatiles and extractables

during coal pyrolysis. These authors report data showing that the yield of pyridine extractables generally goes through a maximum at the temperature at which the rate of volatiles production is highest. In general terms, this coincidence reflects the long recognized fact that in pyrolysis, an initially formed "bitumen" undergoes a disproportionation into a relatively hydrogen-rich volatiles fraction and a hydrogen-poor char fraction. As the temperature at which this disproportionation occurs is passed, the volatiles-forming reactions become progressively more dominated by gas-forming reactions such as dealkylation of small side chains, decarbonylation, and dehydrogenation, and production of large organic volatiles becomes no longer possible. Thus the maximum opportunity for influencing the "disproportionation" process so as to increase the volatiles, and decrease the char will likely come at the point where the natural volatiles formation rate is the greatest, and before rapid H₂ formation squanders whatever hydroaromatic hydrogen is available in the additive or in the coal structure itself. We speculate that the best use of a hydrogen-donor additive in a pyrolysis process, where there is no large confining pressure, will be made by going very rapidly to this temperature region, and then holding the temperature there.

In the rapid heating (1000°C/s) studies of Fong (9), the maximum volatiles formation rate occurred at a nominal temperature of about 600°C, but at the maximum heating rate achievable in the TGA apparatus used in this work (< 7°C/s), the volatiles formation rate was maximum at about 450°C. Therefore, we tested the impact of additives by raising a furnace, previously heated to 900°C, around the quartz tube containing the sample, and when a temperature of 450°C was reached, quickly lowering the furnace. Since the quartz tube cooled slowly compared to the rate at which it was heated, this procedure approximated the desired regimen, but the heating rate was slow enough that blank experiments with the tar additive loaded onto charcoal showed that a large fraction of the tar additive vaporized by the time the pretreated coal reached 450°C.

By comparison, the laser-pyrolysis, with a heating rate of about 10,000°C/s, should bring the pretreated coal to ca. 500°C while most of the additive is still within the coal matrix. Since the temperature of maximum volatiles formation in a linear heating-rate experiment is a function of heating rate, we expect the optimum temperature with laser-heating to be 100 to 200°C above that for the slower heating-rate pyrolysis. Unfortunately, the data shown in Figure 5 were generated when the residence time or "hold time" at maximum temperature was only ~0.1 s, and substantial tar formation is not observed in this short a reaction time unless the final temperature is above 700°C. We chose an upward flow in the pyrolysis cell to move the particles as slowly as practical. However, the distributions of aerodynamic particles sizes used thus far have not been narrow enough to allow successful entrainment at space velocities less than ca. 10 cm/s above the nominal settling velocity of 50-µm coal particles. We anticipate that the use of coal particles having a narrower aerodynamic size distribution, as well as a narrow physical size distribution, will enable us to improve the entrainment and increase the residence time to 0.5 to 1 second, and thus to lower the final pyrolysis temperature substantially.

Characteristics of Laser-Pyrolysis Tars

The tars produced by pyrolysis of the coals in a stream of cold gas, and as collected on the final filter, consist of agglomerates of light yellow spheres, quite evenly sized at about 0.2 to 0.3 µm. Although they contain substantial amounts of rather low boiling materials (e.g., phenol, cresols, etc.), these aerosol particles are not very sticky at room temperature, and do not coalesce when scraped of the filter with a spatula. Upon exposure to air at room temperature, they turn black in several hours.

Several samples of the laser pyrolysis tars have been subjected to FI mass spectrometry. Figure 7 shows the spectra obtained for the tars from the Argonne Pittsburgh No. 8 and Wyodak coals. The volatility of the tars, under the FIMS analysis conditions (heated to 450°C at 3°C/s under a vacuum $\leq 10^{-6}$ Torr) ranges from 57% for some of the Illinois No. 6 tars, to 90% or above for the Pittsburgh No. 8 and Wyodak tars. Since any fossil fuel material that has been through a distillation process (whether atmospheric or vacuum) is typically completely volatile (> 95%) in FIMS analysis, either a substantial part of the Ill. No. 6 tar is ejected as an aerosol without ever being in the vapor phase, or retrograde reactions converted a substantial fraction into non-volatile materials. Since the tars are ejected into a cold, inert atmosphere, where the cooling rate is in excess of 1000°C/s, we judge that any retrograde reactions that did not occur before the tar left the hot coal particle would be unlikely to occur after leaving. Thus the FI mass spectral analyses that are discussed below should be considered representative of the tar as it left the coal particle.

The yields of tars produced in the laser pyrolysis appear, as shown in Table 1, to be about 1.5 times larger than those obtained by Khan et al. (10) in a hot-gas, entrained-flow reactor (hot-tube EFR reactor) with a final temperature of 1100°C. However, uncertainty over what fraction of materials detected in the vapor state (e.g., "olefins") in the work of Khan would be found in the tar from the laser pyrolysis precludes a definitive comparison at this time. Therefore in this report we will focus on some of the differences in the character of the tars produced from the Argonne Pittsburgh No. 8 and Wyodak coals using each of these two rapid-heating entrained-flow pyrolysis techniques. (We reiterate that laser-pyrolysis has no process implications as such. The use of an IR laser in laboratory studies has value insofar as it leads to an increase in fundamental understanding and/or in the ability to improve yields in technologically important processes.)

In general terms, the tars from the Pittsburgh coal are rather similar, whereas those from the Wyodak show some marked differences. For example, in the Pittsburgh tars, the fractions constituted by cresols, dihydroxybenzenes, and the sum of alkylbenzenes and tricyclic alkanes are equal within 30%. However, in the Wyodak tars, the percents of dihydroxybenzenes and the most abundant acyclic alkanes are three and two times larger, respectively, in the laser-pyrolysis tar than in the hot-tube tar. Thus, in the tar that was evolved into a cold gas stream, the abundance of what is presumably the most retrogression-prone class of phenolics -- dihydroxybenzenes -- is substantially higher. What is perhaps more surprising is that the concentration of certain alkanes is also higher in the laser pyrolysis tars. Although there is hardly enough evidence yet to draw a definitive conclusion, a possible rationalization is that when the dihydroxybenzenes (or their precursors) undergo retrograde reactions, they tend to take the some of the alkanes (or their precursors) with them.

A still more striking comparison is that between the FI mass spectra of the laser-pyrolysis tar and that produced from the in-situ pyrolysis of the Wyodak coal in the temperature-programmed inlet of the mass spectrometer (Py-FIMS); the latter is shown in Figure 8. In the spectrum of the laser-pyrolysis tar (Figure 7b) the highest peak among the phenolics (m/z 124, methyl-dihydroxybenzene) and the highest peak of the acyclic alkanes show intensities that are within 40% of each other, whereas in the Py-FIMS, the intensity of m/z 124 is three times that of m/z 268. Because any volatiles produced during Py-FIMS are evolved into a high vacuum, there is negligible opportunity for secondary gas phase reactions; therefore, any increased retrograde reaction under Py-FIMS conditions must be a result of a heating rate that is about three thousand times slower. At this point we cannot say whether the relative enhancement of such retrograde processes is an inherent result of reaction at lower temperatures during the slow heating, or merely reflects a greater chance for retrograde reaction during the slower transport of volatiles once they are generated within the coal.

Comparison of the temperature evolution curves for the most abundant single-ring monohydric and dihydric phenols (xyleneols and methyl dihydroxybenzenes) reveals a rather striking difference between the tars from the two entrained flow techniques. Figures 9 and 10 show that in the laser-pyrolysis tar essentially all of the material in both classes is preexisting in the tar. In the tar generated in the hot-tube reactor on the other hand, most of the monohydric phenols and a good part of the dihydric phenols are pyrolytically generated on the hot probe during the FIMS analysis, as seen from the fact that they are observed at much higher temperature. The difference between the two types of tars is even more pronounced than it appears in Figures 9 and 10, since what is plotted there is the fraction of the total observed in each case for each molecular ion. As shown in Table 1 and discussed above, for the Wyodak coal, the total amount of dihydric phenols in the laser pyrolysis tar is 3.3X higher than that seen in the EFR tar.

The above differences cannot be attributed entirely to a different distribution of volatiles between gases and tars in the two pyrolysis techniques. Since the hot-tube reactor tars were produced by heating the coal to 1100°C and the tars were originally evolved into a hot nitrogen stream, one might have expected the relatively low-boiling phenols to have been much more "distilled" out of the tars during the collection, and a greater fraction of those low molecular phenols that were seen might be expected to have been formed by pyrolysis on the hot FIMS probe. However, in three of the four curves shown, the situation with the laser pyrolysis tars was not merely that there were more preexisting phenols, but that there was essentially no phenol generation during analysis of the laser-pyrolysis tars. Thus we are forced to say that even though one might have expected the higher temperature, longer residence time, and hot-gas atmosphere in the EFR to have produced tars that were more "evolved" and therefore more refractory, they were

not more refractory. It could be that the greater opportunity for oxidative coupling reactions provided by the hot-gas environment of the hot-tube reactor provides coupling products of dihydroxyaromatics that subsequently gave monophenols on the heated FIMS probe. This scenario would be consistent with the substantially lower levels of dihydroxybenzenes seen in the Wyodak hot-tube tars, and also with the higher total tar yields observed in the laser pyrolysis.

In summary, although the chemistry responsible for formation and evolution of oxygenates in coal tars is still largely unknown, the above data from laser pyrolysis in a cold-gas atmosphere are helping to delineate the factors that control the types and amounts of phenolic structures present in pyrolysis products. At this stage, we can make the following tentative conclusions:

- The laser-pyrolysis tar yields appear to be higher than from those produced in hot-tube pyrolysis of the same coals at equal or greater severity.
- The differences between entrained-flow laser-pyrolysis tars and entrained-flow hot-tube pyrolysis tars are much greater for Wyodak coal than for Pittsburgh No. 8 coal.
- The laser-pyrolysis tars contain substantially more low-molecular weight monophenolic and diphenolic structures than do the entrained-flow hot-tube pyrolysis tars.
- These phenolics, which undergo facile oxidation, are presumably responsible for the initial pale yellow tars turning black upon exposure to air.

REFERENCES

1. D. F. McMillen, R. Malhotra, S. E. Nigenda, *Fuel*, **1989**, *68*, 380.
2. D. F. McMillen, R. Malhotra, M. W. Smith, "Cleavage and Crosslinking of Polymeric Coal Structures during Pyrolysis," DOE Quarterly Report, Contract No. DE-AC21-87MC23286, August 1989.
3. R. Malhotra, G. A. St. John, D. S. Tse, D. F. McMillen, *Am Chem Soc, Div Fuel Chem. Preprints*, **1988**, *33(2)*, 257.
4. J. B. Howard, "Fundamentals of Coal Pyrolysis and Hydrolysis," in *Chemistry of Coal Utilization, Second Supplementary Volume*, M. A. Elliott, Ed., John Wiley and Sons, New York, 1982, p. 665.
5. D. F. McMillen, R. Malhotra, S.-J. Chang, W. C. Ogier, S. E. Nigenda, R. H. Fleming, *Fuel*, **1987**, *66*, 1611.
6. R. Malhotra and D. F. McMillen, "A Mechanistic Numerical Model for Coal Liquefaction Involving Hydrogenolysis of Strong Bonds. Rationalization of Interactive Effects of Solvent Aromaticity and Hydrogen Pressure," , submitted to *Energy and Fuels*.
7. D. F. McMillen, R. Malhotra, and D. S. Tse, "Interactive Effects Between Solvent Components: Possible Chemical Origin of Synergy in Liquefaction and Coprocessing," , submitted to *Energy and Fuels*.
8. See, for example: M. M. Boduszynski, *Energy and Fuels*, **1987**, *1*, 1
9. W. S. Fong, W. A. Peters, and J. B. Howard, *Fuel*, **1986**, *65*, 251.
10. M.R. Khan, M. A. Serio, R. Malhotra, and P.R. Solomon, *Am. Chem. Soc. Div. Fuel Chem. Preprints*, **1989**, *34(4)*, 1054.

Table 1
 YIELDS OF TAR AND SELECTED PHENOLIC AND ALIPHATIC COMPOUNDS
 IN LASER- AND HOT-TUBE¹-COAL PYROLYSIS

Coal	Pyrolysis Technique/ Run No.	T _{final} °C	% Tar Yield ²	Tar/ Char	% FIMS ³ Volatility	% Total Ion Intensity ⁴			
						m/z			
						122	124	260	268
WYODAK (Argonne)	LP/6-8-89-3	750	17.4	0.28	90	0.18	0.77	0.43	0.63
Pitts No. 8 (Argonne)	LP/6-13-89-2	925	27.4	0.64	92	0.11	0.11	0.38	0.24
ILL No. 6 (Argonne)	LP/5-26-89-1	880	29.2	0.57	71	0.13	0.29	0.36	0.34
WYODAK (Argonne)	HT	1100	7.71	0.18	86	0.067	0.23	0.31	0.32
Pitts No. 8 (Argonne)	HT	1100	21.84	0.46	63	0.075	0.057	0.18	0.30

¹Data taken from the hot-tube entrained-flow pyrolysis results in Reference 10.

²In LP, % tar yield is derived from the collected weights of tar and char, by assuming the same gas yield reported in the 1100°C, hot-tube pyrolyses of reference 10. This gas yield will be an over-estimate, because of both the lower final coal temperatures of the LP runs and the cold gas atmosphere in the laser pyrolysis.

³Wt. % volatilized from probe at 450°C under high vacuum.

⁴m/z 122 corresponds to methyl cresols, 124 to methyl dihydroxybenzenes, 260 nominally to tetra-cyclic alkanes and alkyl-benzenes, and 268 nominally to acyclic alkanes. The % ion intensity values do not exactly equal mole %, owing to differences in sensitivity factors. However, the relative % changes in intensity values from one sample to another are expected to be reliable.

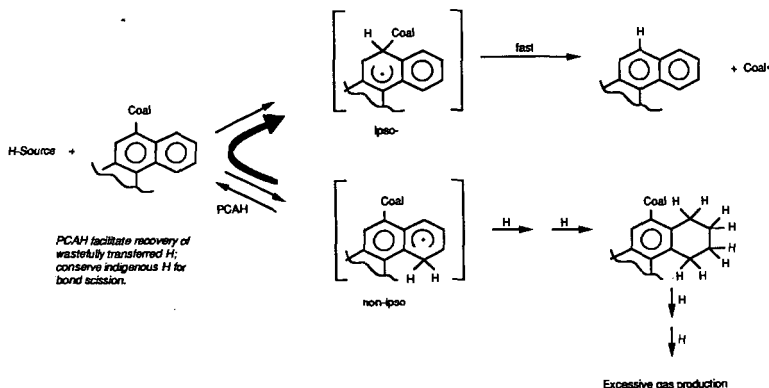
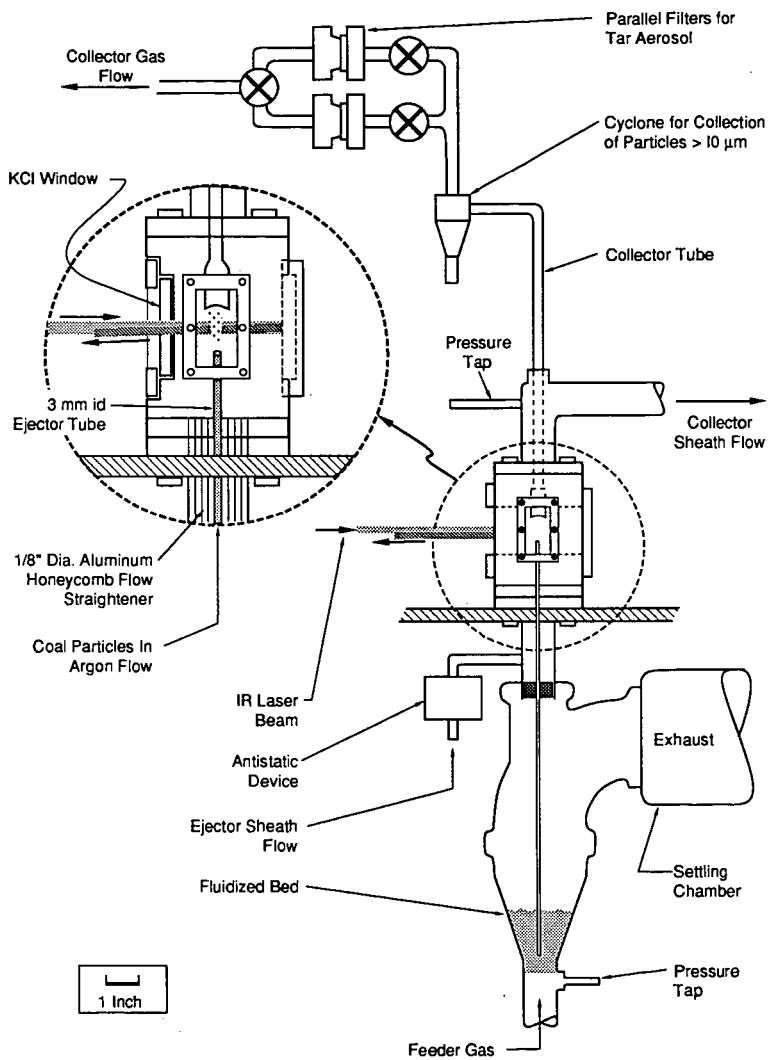


Figure 1. Rationale for Using Additives Rich in Polycyclic Aromatic Hydrocarbons (PCAH).

Premises: 1. Significant contribution of Induced bond cleavage.

2. Factors enhancing IBS also tend to minimize retrogressive reactions.



RA-M-4159-2

Figure 2. Schematic of entrained-flow laser pyrolysis apparatus.

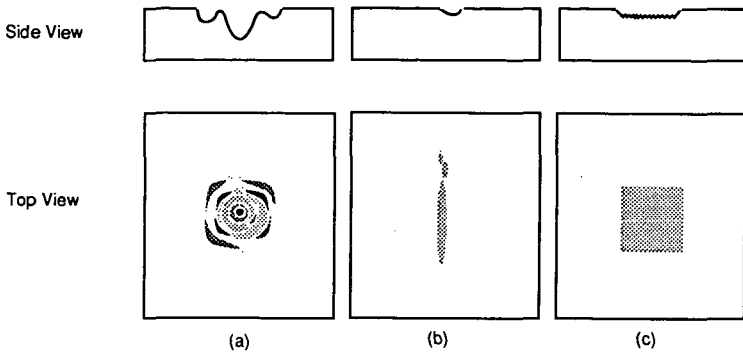


Figure 3. Schematics of burn patterns produced in acrylic pieces using (a) apertures, (b) beam expander, or (c) channel integrator in the optical configuration.

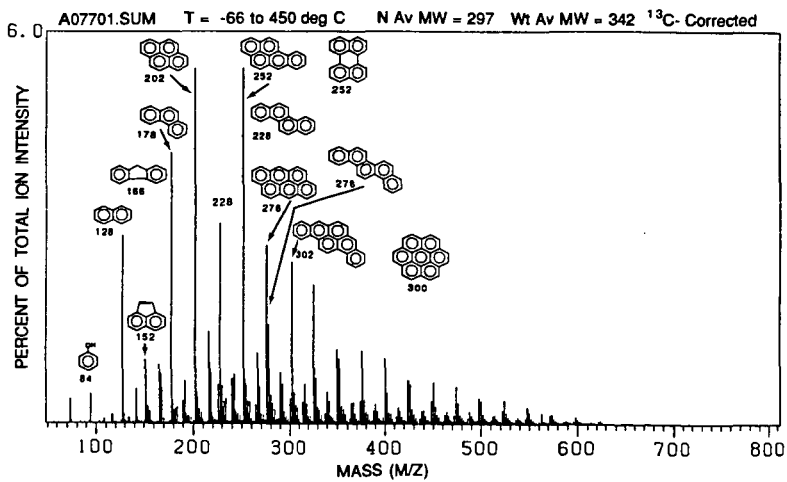


Figure 4. Field ionization mass spectrum of the coal tar prior to hydrogenation. Note that the tar is rich in PAH essentially devoid of alkyl substitution.

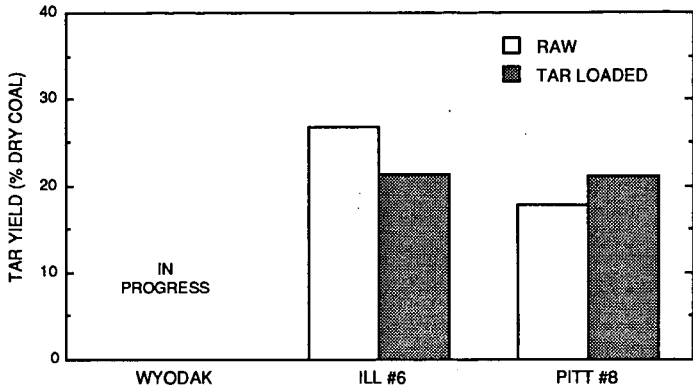


Figure 5. Effect of loading hydrogenated coal tar on the tar yield during laser pyrolysis. Maximum temperature of about 880°C for the ill. #6 coal and 840°C for Pitt. #8 coal.

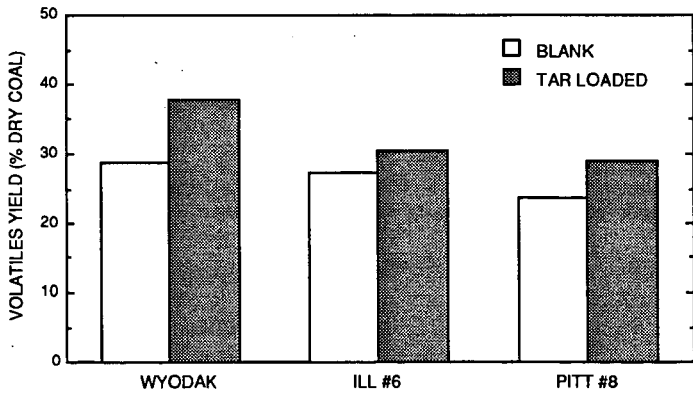
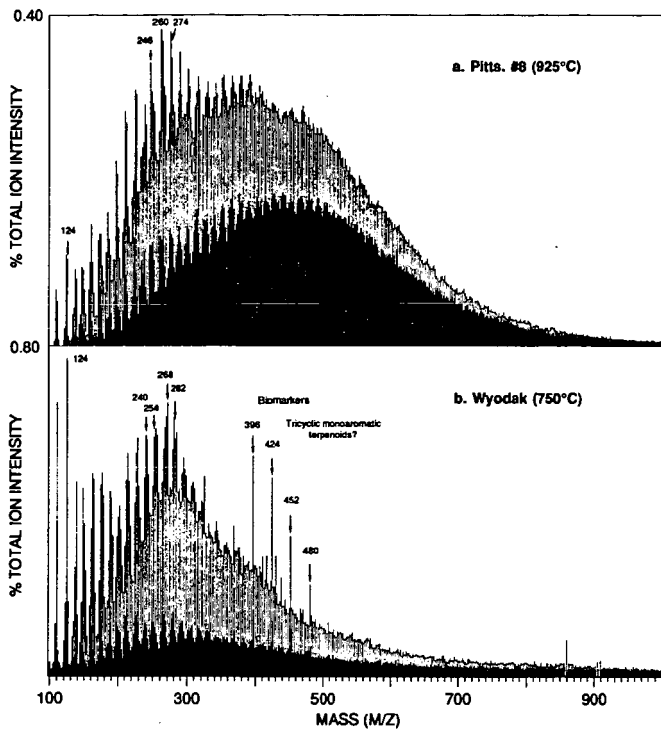


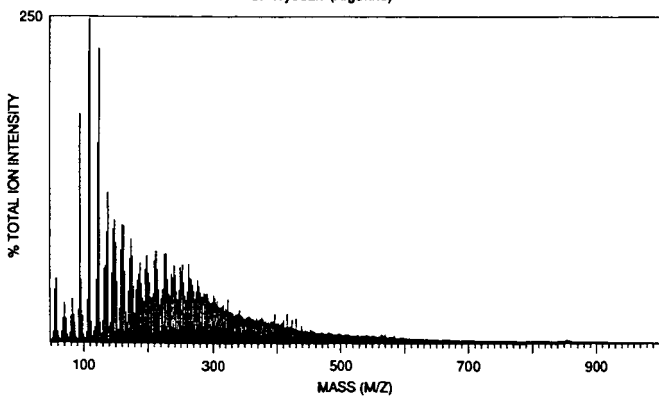
Figure 6. Effect of loading hydrogenated coal tar on volatiles yield during vacuum pyrolysis to a maximum temperature of about 450°C.



RA-4159-3

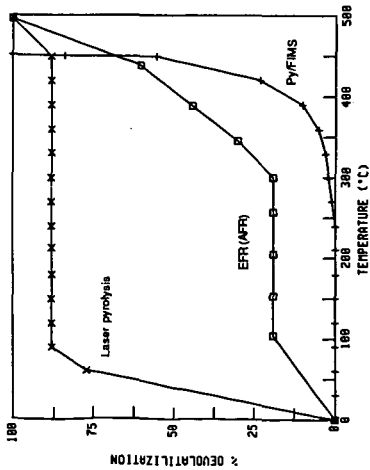
Figure 7. FI mass spectra of laser pyrolysis tars.

- a. Pittsburgh No. 8 (Argonne)
- b. Wyodak (Argonne)



RA 4159-4

Figure 8. Py-FIMS of Wyodak coal (Argonne Premium Coal Sample Program).



466

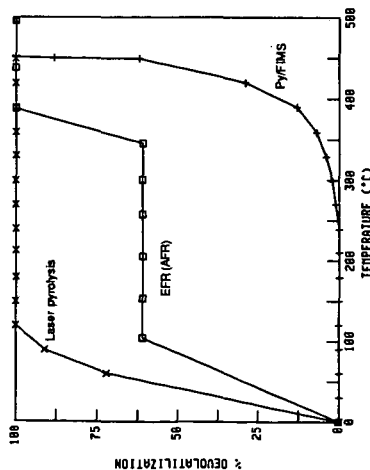


Figure 9. Temperature evolution profile of phenolics during FIMS analysis of laser-pyrolysis tar and tar from entrained flow pyrolysis in a hot tube (EFR), compared with the evolution during in-situ pyrolysis in the FI-mass spectrometer (Py-FIMS) of the Argonne Pittsburgh No. 8 coal. (a) monohydric phenols (m/z 122); (b) dihydric phenols (m/z 124)

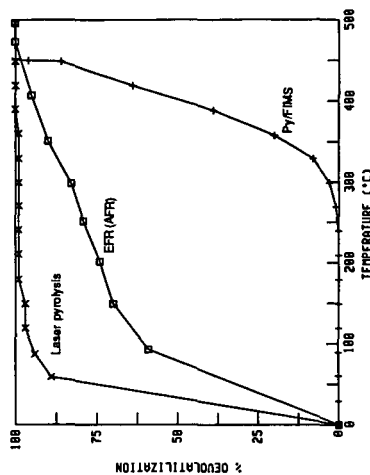
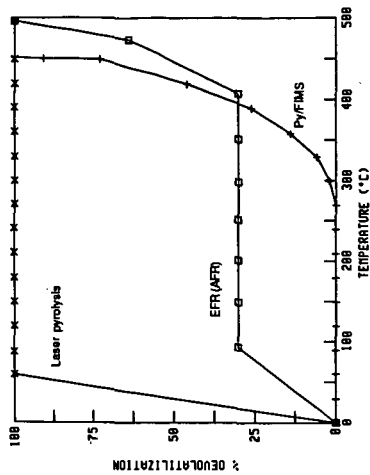


Figure 10. Temperature evolution profile of phenolics during FIMS analysis of laser-pyrolysis tar and tar from entrained flow pyrolysis in a hot tube (EFR), compared with the evolution during in-situ pyrolysis in the FI-mass spectrometer (Py-FIMS) of the Argonne Wyodak coal. (a) monohydric phenols (m/z 122); (b) dihydric phenols (m/z 124)

CHARACTERIZATION OF COAL BY PYROLYSIS

A. Björkman and P. Simonsen
Technical University of Denmark
Lyngby, Denmark

1. Introduction

Coal characterization is an old subject. The heating value is a major important figure from an economic point of view. The common classification in ranks, however, has been associated with the coking properties and is usually based on the volatile matter content. Its value for the firing (and gasification) of coals is limited. One indirect method - vitrinite reflection is based on petrographic correlation. Also DTA and TG measurements are studied, but have not gained much use as yet.

The annual report 88/89 of IEA Coal Research gives some comments on the matter, stating that characterization should identify properties, that are critical to the performance of the coal. There is a need for better evaluative tests, based on modern techniques, but it is considered unlikely that methods can be devised in the near future, which are both specific, good for all coals and still simple.

Considering these methods and other characterization measurements, which are mainly analytical, it may be stated, that no method does really try to relate measured properties of coal with its burning characteristics, except for the somewhat primitive "drop-tube burning". Studies of the behaviour of coal particles in flames - usually contrived as some pyrolysis/gasification model - can be considered as characterization but may not easily produce figures for inherent coal properties.

The suggested approach, presented here, emphasizes pyrolytic properties of coal. A small sample is subject to a rapid well controlled laser-induced pyrolysis, followed by an equally controlled gasification, using a microbalance, to estimate the reactivity of the char, formed by the pyrolysis. The principal aim is not to contribute to the fundamental understanding of coal burning but to add - by the use of advanced equipment - to the empirical comprehension of burning properties of coal.

The purpose of the proposed measurements is thus related to the pyrolysis and gasification, which occurs during practical firing, where the time and intensity of pyrolysis may vary considerably between coal particles. The way a particle responds to pyrolysis is known to influence the char reactivity and may thereby determine the final burning (gasification). The approach presented here is apparently not attempted before.

The use of a very small sample is necessary to achieve a rapid pyrolysis with a laser beam, which in turn necessitates the use of a microbalance for the gasification step.

2. Equipment and procedure

Sample preparation

Coal powder (< 270 mesh) is pressed to a thin disc (< 0.1 mm) and cut to a circular specimen (4.5 mm), which is laid in a tiny quartz glass crucible and its weight recorded. It was established experi-

mentally, that the thickness of the specimen must be restricted to a maximum thickness of about 1 mg.

Rapid pyrolysis

The sample crucible is placed in a pyrolysis chamber (Fig. 1), which is flushed with pyrolysis atmosphere (usually He), and possibly pressurized. A glass window allows radiation of the sample with a laser beam, and a portion of the resulting gas may be sampled through a rubber septum, using a syringe.

A Neodym/YAG laser has been used, giving a beam, coaxial with sample and having the same width. The beam energy could be increased up to 14 J and given 1 to 20 ms duration. The pyrolysis gas was analyzed in a Perkin Elmer 8500 gaschromatograph with double detectors, combined to monitor for H_2 , CO, CH_4 (conjunct), C_2H_2 , C_2H_4 , C_2H_6 and C_3H_6 .

About 90% of the tar formed did deposit on the crucible wall, but no attempt was made to analyze or characterize this product. It would have been a difficult undertaking as such and could not be accommodated in the project.

Reactivity rating

The char disc (about 1 mg) from pyrolysis can easily be transferred to a clean crucible. It is vital that this crucible is handled carefully to avoid any generation of static electricity. The char is covered with a thin layer of quartz wool to assure that no char (or ash) is lost.

The gasification is made in a (locally built) apparatus, seen in Fig. 2, which is for the most part selfexplaining. A Satorius electronic ultramicrobalance (type 4436 MP8) has been used. It is important that the filament (steel + Pt), which carries the char crucible, is centered to avoid any contact to the furnace wall. It is also important to avoid any movement of the balance, when the hanging furnace is heated, which explains the use of an expansion joint. A small stream of nitrogen is used to protect the balance and to keep an unchanged atmosphere around the counterweight.

A partly perforated mixing section at the furnace top protects the filament and gives complete mixing of the two gas streams. Temperatures up to 950°C for H_2O or CO_2 could be used but most experiments were run (with O_2/Ne) at about 430°C. The temperature variation in the furnace chamber could be kept within 1°C.

After insertion of quartz crucible, the gasification is started with extended flushing of the furnace with N_2 before turning on the heating. The temperature rise was normally quite rapid, but not until after about 2 hrs. the temperature became stable and the reactant gas could be admitted. The gasification media (O_2 , H_2O , CO_2) were diluted with N_2 .

During the introductory phase of the experiments it was found to be proper to normalize the amount of char gasified at any time to the maximum amount possible. This latter value was found by raising the temperature of the oven 200°C in a flow of nitrogen, whereafter the oxidation is completed within few minutes to constant weight giving the ash figure.

3. Experimental results

Of the introductory/guiding experiments only a few need to be reported. Reproducibility of the two-step procedure was found to be quite satisfactory. The rate of gasification did not change when the flow of reactant gas was reduced to half, and the rate seems to be directly proportional to the O_2 concentration (25 and 50%). Rate values at comparable conditions in the temperature range 408–438°C gave activation energies in the region 120–150 $\text{kJ}\cdot\text{mol}^{-1}$, indicating that reaction rate only is rate-controlling.

A comparison of the relative rating of two coal samples is shown in Figures 3 to 5, using O_2 (65%), H_2O (29%) and CO_2 (50%). When the differences in curve heights are compared at the same degrees of gasification, the H_2O and CO_2 ratings are nearly the same, while the "separation" is somewhat larger for O_2 . H_2O is, however, more reactive than CO_2 . The use of O_2 is preferred, since the lower temperature is lenient to the furnace.

Using one coal sample, the influence of pyrolysis time at the same laser energy input (12 J) on rate of gasification was measured (Fig. 6). While the amount of pyrolysis residue (char) did not vary much, it is evident, that the reactivity of the char gets considerably higher, when pyrolysis time is short. This effect is likely to increase the spread of burning times in a PF flame.

The effect of laser energy input at constant pulse length (1 ms) was also studied. As seen in Fig. 7 the samples with the smallest amount of energy start at a lower degree of pyrolysis but are somewhat more reactive, why the final level of gasification gets to be more or less the same.

In another study with a set pulse time the ratio of energy to specimen weight was kept constant (Fig. 8). It resulted in almost identical gasification curves.

The composition of the pyrolysis gas varies somewhat with the laser-pulse duration as shown in fig. 7. These values may not be important for combustion performance but could give an indication of pyrolysis properties. When the level of laser energy was varied at constant pulse length the following relative amounts (μl) were formed:

Energy, J	1	2	5	10
H_2	32	88	122	139
CO	9	31	57	81
CH_4	1.2	1.4	1.7	2.3
C_2H_4	0.43	0.46	0.73	1.15
C_2H_2	1.9	5.5	19.6	3.6

The rise in amounts was particularly strong in the lowest range of energy increase, except for C_2H_2 .

From the curves shown so far and several others it can be inferred, that the (relative) amount of "post-pyrolysis" is proportional to the reactivity of the char, expressed as the initial slope of gasification curve.

In the Figures 10 to 13 some pyrolysis and gasification curves are given for the following 4 coal samples within the same rank, the figures being in %:

Origin	H ₂ O	Ash	Volatiles
Australia	2.2	16.1	37.3
Mozambique	2.8	10.1	40.0
South Africa	2.9	13.3	29.9
Poland	2.6	17.2	38.4

It may be stated generally from the "reactivity curves", that the new type of characterization does discriminate between different coals. The differences appear as ultimate levels of (normalized) residue and as response at changes in pyrolysis parameters. It would be of interest to understand how these differences may be explained, but the important matter is to relate the observations to the performance of the coals in practical burning.

Fig. 13 also illustrates the deviation in behaviour, when the pyrolysis is done by heating the coal specimen slowly in the gasification oven. Evidently the slow carbonization yields a reactive char, which has almost the same "gasification profile" as the char from a low energy laser pulse (1 J) of short duration (1 ms). However, in characterization laser pyrolysis is more realistic and easier to control.

Though the use of CO₂ as gasification medium is less attractive, it is of fundamental interest to check the influence of characterization parameters in comparison to O₂. It was found as a main observation, that the difference in reactivity, resulting from short and long pulse lengths, seems to be considerably smaller on CO₂ gasification.

Several experiments were made with different atmospheres and increased pressures in the pyrolysis chamber. On the whole, the effects observed were rather insignificant. Also a splitting of the laser energy into several consecutive pulses seems to give additional information of interest. *Title*

A few experiments with particles of different ranges in the coal powder, used to press the disc specimen, indicate some differences in the reactivity of the produced chars. Evidently, the particle size distribution should be controlled in accurate work.

Finally two series of "characterization experiments" were carried out, one with coals of different ranks, the other a comparison with results, produced by the Danish service and research institute dkTEKNIK.

The first series comprised one subbituminous coal (West Canada), two bituminous coals (South Africa), one "in between" these ranks (Columbia) and, as the last, anthracite. The laser energy was kept constant while two pulse lengths (1 and 20 ms) was used. The results are shown in Figures 14 and 15. The 1 ms experiments give a clear discrimination between the ranks, and the two bituminous coal appear to be identical. However, the 20 ms experiments do distinguish between these two coals, while the ranking order of the most reactive coal chars gets "mixed". Generally the new characterization method appears to be quite efficient.

The second series illustrates the only comparison with results from practice, identified so far. The three coals involved have the following conventional data:

Coal from	Ash,%	Volatiles,%	H _i kcal/kg	Softening temp.,°C
Poland	16.1	36,0	7749	1190
South Africa	12.8	28,8	7783	1340
Mozambique	17.6	36.9	7690	?

Petrographic figures show substantial differences in vitrinite and inertinite contents. The DTH/DTC/TG data seem to differ moderately and do not offer an easy interpretation. The following test results are at hand (only two coals being used in PF firing):

Coal from	Drop tube % burnt	Ignition, combustion	Not burnt in ash,%
Poland	96,1	very good	2
South Africa	87,8	rather good	6
Mozambique	94,4	-	-

The overall dkTEKNIK results grade the samples in the order: Poland, Mozambique, South Africa. The pyrolysis/reactivity results, as shown in Fig. 16 give the same order. A detailed comparison does not seem possible.

4. Summary

The results obtained do meet the prospects of a new possibility for coal characterization, in that the proposed principle seem to have a definite potential of practical interest. The method displays good reproducibility and reflects also minor differences in coal properties. The number and ranges of significant parameters appear to be limited, and standardization to optimal conditions, e.g. with regard to laser requirements, should be possible, using simplified equipment.

We have been invited by the European Common Market Authorities to examine the possible development of a commercial apparatus with the support of consultants with experience of such endeavours.

Lyngby, December 1989

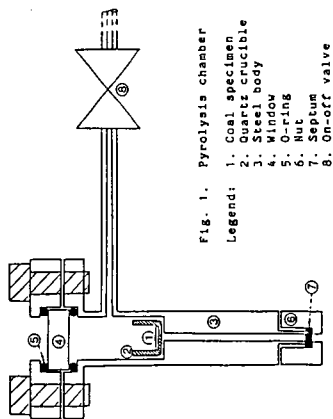


Fig. 1. Pyrolysis chamber
 Legend:
 1. Coal specimen
 2. Quartz crucible
 3. Quartz body
 4. Window
 5. O-ring
 6. Nut
 7. Septum
 8. On-off valve

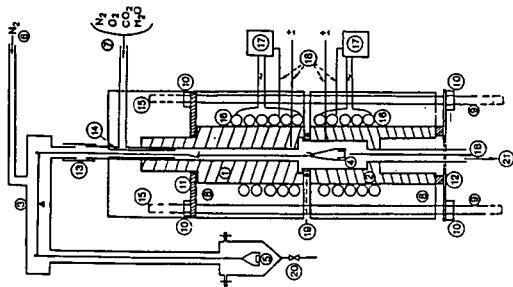
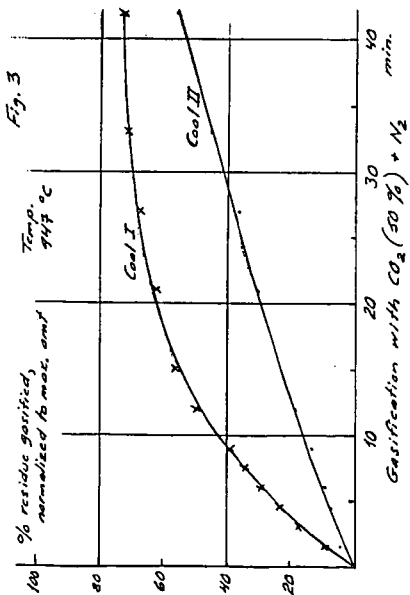
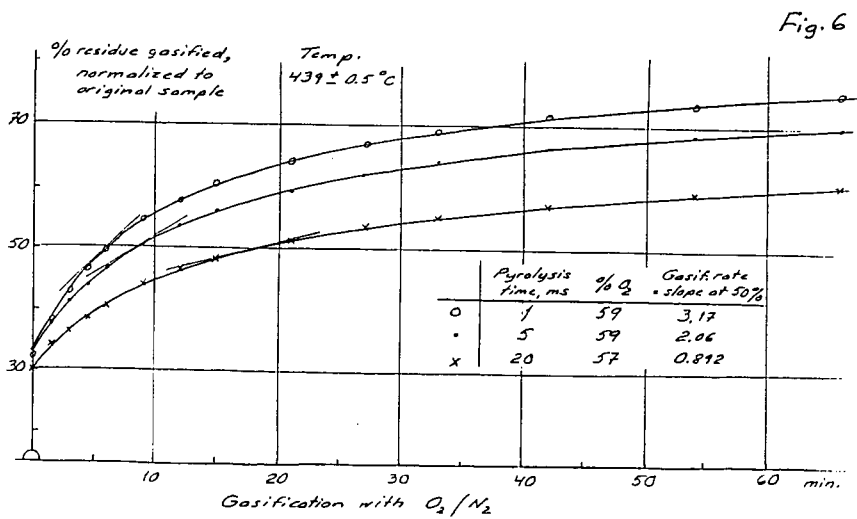
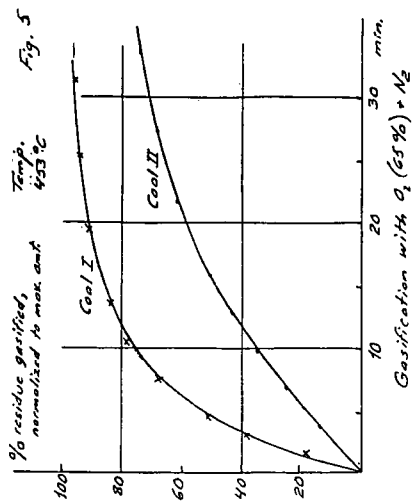
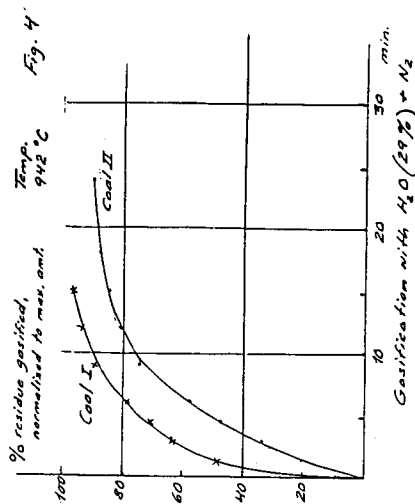


Fig. 2. Reactor furnace and microbalance
 Legend:
 1. Reactor body, upper part } heat resisting steel
 2. Reactor body, lower part }
 3. Micro balance
 4. Weighing pan (carrying crucible with coal specimen)
 5. Weighing pan (with specimen)
 6. H₂ inlet (for protection of balance)
 7. Inlet for N₂, O₂, CO₂, H₂O
 8. Insulation
 9. 4 steel bars (to keep reactor parts together)
 10. Bolting nuts
 11. Top plate
 12. Top plate (springy material)
 13. Expansion joint
 14. Mixing section
 15. Prolonged bars (acting as hanging support)
 16. Heating coil
 17. Temperature controls
 18. Thermocouples
 19. Packing
 20. Vent
 21. To cooler and chromatograph





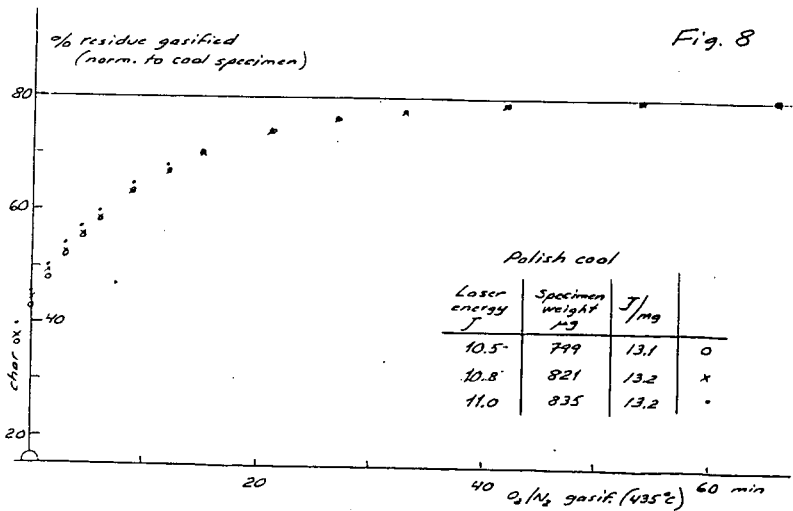
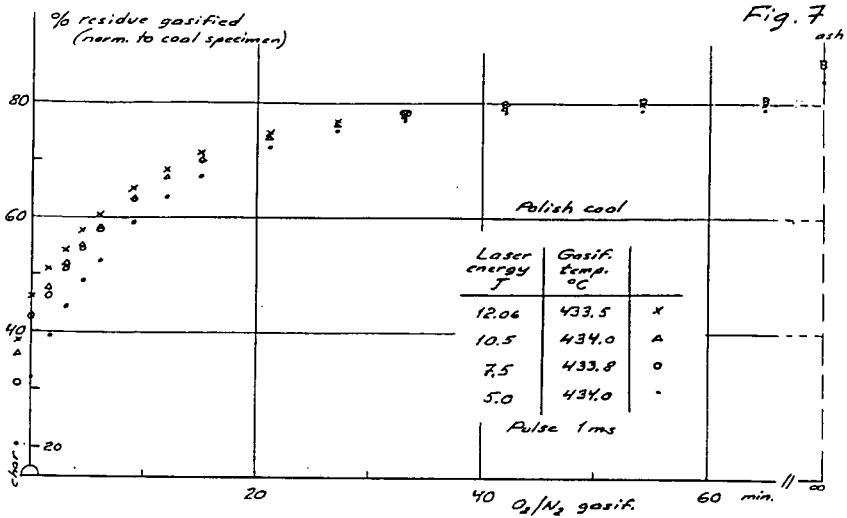
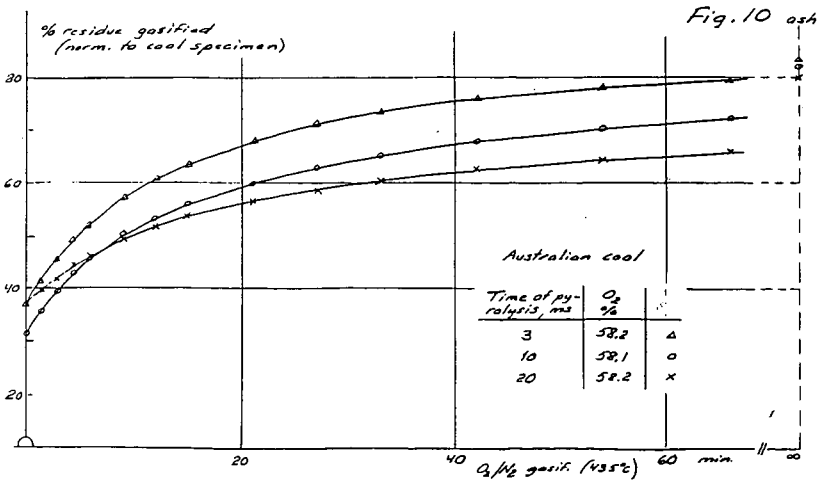
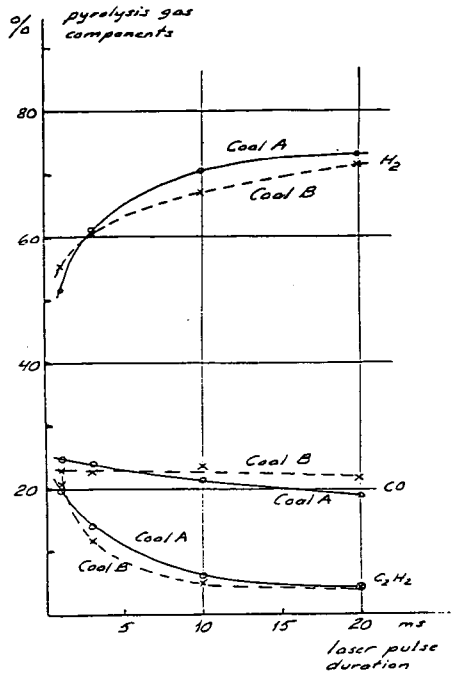
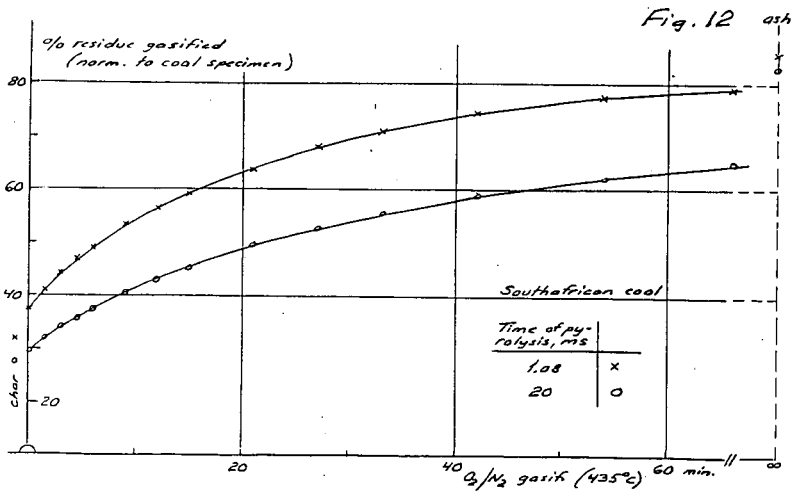
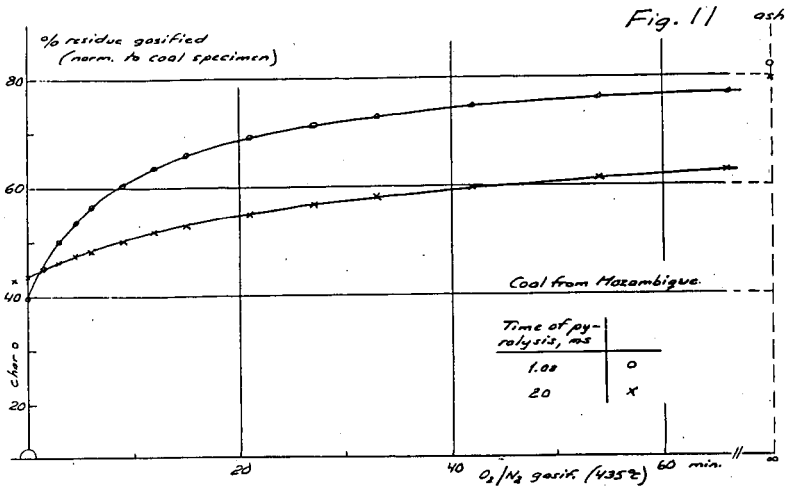
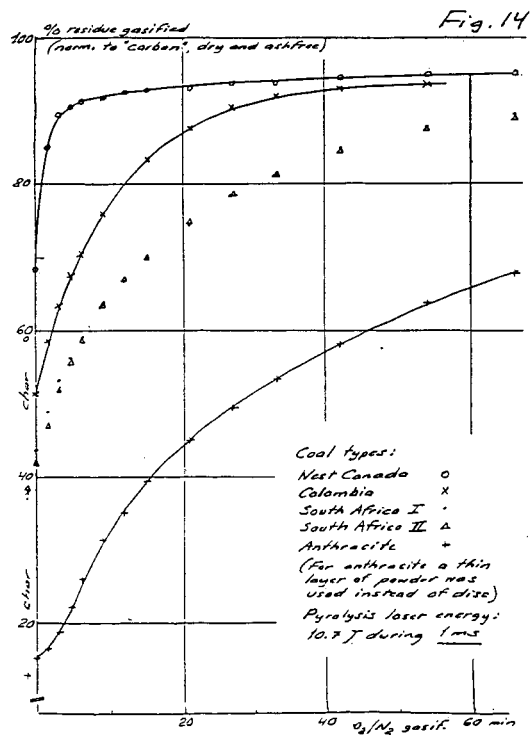
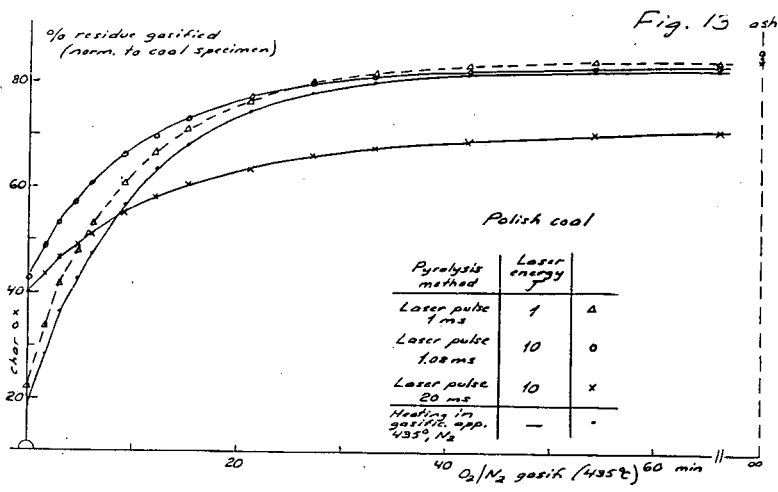
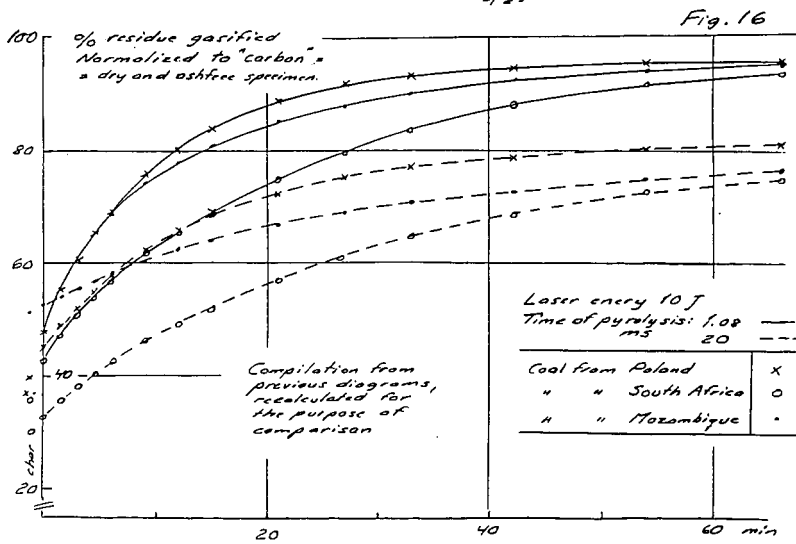
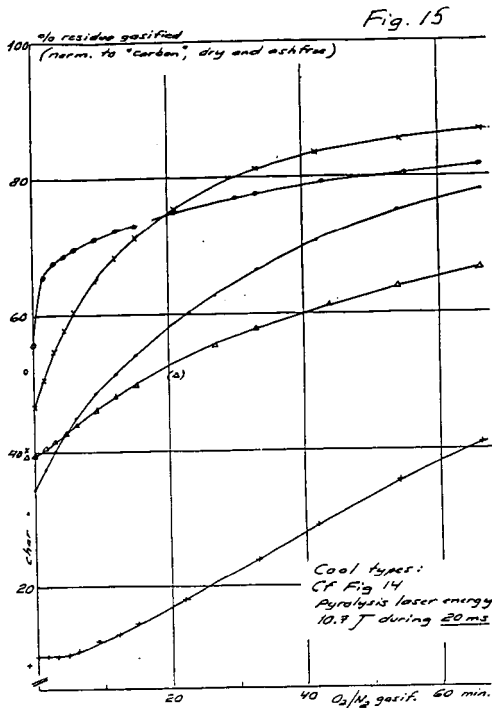


Fig. 9









ADVANCES IN THE FG-DVC MODEL OF COAL DEVOLATILIZATION

P.R. Solomon, M.A. Serio, D.G. Hamblen, Z.Z. Yu, and S. Charpenay
Advanced Fuel Research, Inc., 87 Church Street, East Hartford, CT 06108

KEYWORDS: Coal, Pyrolysis, Modeling, Network, Kinetics

INTRODUCTION

The FG-DVC general model for coal devolatilization, which combines a functional group (FG) model for gas evolution and a statistical depolymerization, vaporization, and crosslinking (DVC) model for tar formation, has previously been presented (1). The FG model describes the evolution of gases from sources in the coal, char and tar. The DVC model describes the decomposition and condensation of a macromolecular network representation of coal under the influence of bond breaking and crosslinking to predict (using Monte Carlo statistical method) the molecular weight distribution of the network fragments. The crosslinking reactions are related to the evolution of CO₂ at low temperature and CH₄ at moderate temperature (2). Tar is formed from the light fraction of the network fragments which vaporizes and is transported by the light gases.

As discussed in Ref. 1, the FG-DVC model was based on a number of simplifying assumptions which provided a good first approximation of the devolatilization process. Included in the approximations were the assumptions that: i) the coal molecular structure could be described as substituted aromatic ring clusters of various sizes linked into a macromolecular network or present as guest molecules, ii) tar consists of fragments of that network and so has a similar composition. (except for a higher hydrogen content due to a larger number of methyl groups), iii) kinetics are independent of coal rank, iv) transport is controlled by the vapor pressure of tar fragments in the escaping gases.

Since the presentation of the original FG-DVC model, a number of improvements have been made. First we have added a second class of material, polymethylenes, to the macromolecular network. These polymethylenes can form a large part of the tar in low rank coals and so make the tar dissimilar to the parent structure (which is primarily the aromatic ring clusters). Second, the molecular weight distribution of macromolecular network fragments has been used as the basis for a theory of viscosity (3). This theory is quite sensitive to the accuracy of the kinetic rates. Consequently, third, rank dependent kinetics have been added to the model (3,4). Fourth, we have tested the tar transport theory by comparing its predictions on molecular weight distributions to measurements made with a Field Ionization Mass Spectrometer (FIMS). The results suggest that the vapor pressure law (5) used in the original model (1) appears to fit the data in its dependence on molecular weight and temperature, but was about a factor of 10 too low in its vapor pressure. Finally, we are exploring the use of percolation statistics as an alternative to the Monte Carlo calculations. An approximation is presented which includes the evolution of tar molecules and is based on a previously presented two coordination number percolation theory (6).

MODEL IMPROVEMENTS

Polymethylenes

Varying amounts (typically 0-9%, but in some cases as high as 18%) of long-chain aliphatics (polymethylenes) have been reported in pyrolysis products by Nelson (7) and by Calkins and coworkers (8-11) and references quoted therein. The chains appear alone and attached to aromatic nuclei. The presence of these polymethylenes makes the tar more aliphatic than the parent coal. Also, for most coals, there is a low temperature tar peak which results from the vaporization of unattached small polymethylenes plus small aromatic ring clusters. This vaporization peak is illustrated in Fig. 1. Polymethylene chains can also crack or be released into the second tar peak. Further cracking of this material under more severe devolatilization conditions produces ethylene, propylene, and butadiene from which the concentration of polymethylenes may be determined (11). Originally, the polymethylenes were included in the FG model as part of the aliphatic functional group pool, which is assumed to decompose to produce gas products, not tar. This leads to predicted H/C ratios in the tar for low rank coals which are lower than those measured by Freihaut et al. (12).

Polymethylenes have now been added to the DVC part of the model as a second class of material whose molecular weight distribution and functional group composition are different from the main macromolecular network. The starting coal molecule now includes a distribution of oligomer sizes for polymethylenes and other guest molecules (with the chemical composition of the network). The vaporization of these molecules produces a peak which matches the early vaporization peak as shown in Fig. 1. We also account for polymethylenes which are attached to the coal matrix and removed by bond breaking by including them as species in the FG model. Those polymethylenes are then added to the tar after vaporization.

The model requires a value for the total polymethylene content in the coal. Calkins determined that the yields of ethylene, butadiene, and propylene correlated well with the polymethylene content (11). It was decided that this is the most general and fruitful approach to take and we have used the coals which are in our set and Calkins' set to calibrate the method. As a first approximation, we arbitrarily chose to use polymethylene = 0.7 (C₂H₄). This gave -CH₂- contents slightly above Calkin's values, but within 15% of Calkin's. The model also assumes that 50% of the polymethylenes are small enough to vaporize and are included in the oligomer pool while the other 50% are not and are included in the FG pool.

A prediction for the total tar yield including polymethylenes is compared in Fig. 1 with measurements from a TG-FTIR experiment (13-15). The agreement is good. Comparisons between the predicted and measured (12) tar hydrogen compositions are shown in Fig. 2. The prediction is good for high rank coals and shows the correct trend with rank. The tar hydrogen composition is, however, overpredicted for lower rank coals. This is due to the fact that the model underpredicts, for these coals, the tar yield at high heating rates. The relative contribution of polymethylene is then more important. By improving the tar prediction with adjustments of DVC parameters, we should be able to obtain more accurate values of the tar hydrogen composition.

Viscosity Model

We have developed a model for coal fluidity as an extension of the FG-DVC model (2). The FG-DVC model predicts the yield of liquids (all fragments released from the network) produced during heating of the coal. The fluidity is dependent on the relative amounts of the liquid, and solid (the remaining network) and on the fluidity of the liquid component. The fluidity of the liquid component depends on the average molecular weight of the liquid and on the temperature. The details of the fluidity model and comparisons to literature values of viscosity are presented in Ref. 3. Excellent agreement has been obtained between the model predictions for fluidity and low temperature fluidity measurements of Oxley and Pitt (16), Fitzgerald (17), and van Krevelen (18).

Recently, we have applied the model to predict the fluidity data for the Argonne premium samples obtained using a Geissler plastometer (19). To properly predict the fluidity we found that the rank independent kinetics were no longer accurate enough. Rank dependent rates for bond breaking, low temperature crosslinking, and moderate temperature crosslinking were determined using the evolution rates for tar, CO₂, and CH₄ in a TG-FTIR experiment as discussed in the next section. Their rank dependent rates were used to make the predictions of viscosity.

Figure 3 compares the measured and predicted viscosity for Upper Freeport coal. Figure 4 shows the predicted and measured values for the temperature of the initial softening point (where the plastomer first reads 1 DDM), the temperature of maximum fluidity, the maximum fluidity value, and the solidification temperature (where the plastometer last reads 1 DDM). The agreement is good, generally within $\pm 10^\circ\text{C}$ for the temperature predictions and within a factor of 5 for the fluidity maximum.

Rank Dependent Kinetics

As discussed above, in order to fit the fluidity data, the tar formation, carbon dioxide, and methane kinetic rates had to be adjusted from those used in the original model which were rank independent (1,20). These rates control the bridge breaking, low temperature crosslinking and moderate temperature crosslinking rates, respectively. The rank dependent rates were chosen by fitting the TG-FTIR data at 30°C/min and the Geissler fluidity data (19) at 3°C/sec.

In addition to this study, an independent investigation was made of the rank dependence of the pyrolysis kinetics by doing experiments in a TG-FTIR reactor over a series of heating rates (3, 30, 50, 100°C/min) for the Argonne coal set (4).

The rank dependences of the rate constants for bridge breaking, (or tar evolution) and CH₄ evolution at 450°C determined from analyzing the TG-FTIR data at several heating rates and from fitting the FG-DVC model to fluidity data at 3°C/min and the tar and methane evolution data at 30°C/min are shown in Fig. 5. The two methods agree fairly well and show a systematic variation in rates with the coal's oxygen concentrations. The rates for tar evolution or bridge breaking vary by about a factor of 10 if the Pocahontas coal is excluded, which is consistent with previous results for coals from the same range of ranks (21). If the Pocahontas is included, the rank variation for the tar evolution or bridge breaking rates is about a factor of 25. The rates for tar evolution are consistent with those obtained by Burnham et al. (22) for total hydrocarbon evolution from Rock Eval analysis of the same coals.

Tar Transport Model

The tar transport model assumes that the tars reach their equilibrium vapor pressure in the light gases and evolve with these gases as they are transported through the pores or by bubble transport. The details of the model are presented in Ref. 1. We have used the vapor pressure correlation of Suuberg et al. (5) for the equilibrium vapor pressure. Since this vapor pressure law is a function of molecular weight and temperature, we tested the accuracy of our model in predicting the evolution of tar fragments of specific molecular weight as a function of temperature.

The experimental data used was obtained from FIMS analysis, where the FIMS apparatus is in line with a probe used to heat the sample. The FIMS analysis was performed by Ripudaman Malhotra at SRI International on coals, which pyrolyze in the apparatus (coal FIMS), and on already formed coal tar, which vaporizes in the apparatus (tar FIMS). We divided the tar oligomers (from both data and theory) into five different bins: 50-200 amu, 201-400 amu, 401-600 amu, 601-800 amu, and > 800 amu. The evolution with temperature of each bin is then plotted.

Tar FIMS - We found good agreement between the tar FIMS data and our simulation (Fig. 6). A small mismatch is present for large molecular weight oligomers (> 800 amu), where the maximum of rate evolution occurs later in the simulation. The peak is also narrower, i.e. the temperature range of evolution is shorter than found experimentally. The vaporization of smaller oligomers is, however, well predicted. This validates the temperature and molecular weight dependence of the vaporization law (5) used in the model but not the absolute magnitude of the vapor pressure.

Coal FIMS - We compared the results of the simulation with coal FIMS data for two coals, Pittsburgh No. 8 and Wyodak. We found the best agreement when the Suuberg et al. correlation (5) is multiplied by ten. For the Pittsburgh No. 8, the theory gave an accurate prediction for the evolution temperature of low molecular weight oligomers, as well as the relative amounts of all oligomer classes (Fig. 7). It, however, predicted higher evolution temperatures for high molecular weight oligomers (> 600 amu), while the data showed a unique temperature of maximum evolution rates (T_{max}) for all molecular weights. A shift to higher T_{max} with higher molecular weight is consistent with the fact that large oligomers need higher temperatures to vaporize, as confirmed by the tar FIMS data. Since coal FIMS data doesn't present this feature, we suspect some additional limitations occur as the fluid coal melt resolidifies.

The simulation for Wyodak coal gave a good prediction for the evolution of all molecular weight classes oligomers, including large ones (Fig. 8). The data (Fig. 8b) shows that the evolution of high molecular weight oligomers occurs slightly before the smaller oligomers. This also suggests the presence of additional limitations. In our simulation for low rank coals, the peak position is regulated by the low temperature cross-linking rate (which reduces the number of large oligomers which can vaporize) rather than by the vaporization law.

In order to obtain a better prediction for Pittsburgh No. 8, we considered additional transport limitations related to the reduction in the fluidity of the coal. However, none of the simple modifications tried gave a significant improvement in the model for both low and high rank coals. The current model gives good predictions for the relative amounts of the oligomers in each size classification. It also predicts accurately the evolution temperature of low molecular weight (< 600

amu) oligomers. The vapor pressure dependence on temperature and molecular weight is also validated by the good prediction of the tar FIMS data. The present model, therefore, uses the original FG-DVC transport assumption (1) with the Suuberg et al. vapor pressure correlation (5) multiplied by ten.

Percolation Theory

The statistical Monte Carlo method used in our FG-DVC model has been quite successful in predicting the depolymerization and crosslinking processes of the coal macromolecular network. However, the method has a few drawbacks. First, it is computationally time-consuming compared with other statistical methods. Second, its statistical nature presents a certain degree of fluctuation in the final results. The latter becomes increasingly significant and poses some difficulties for the modeling of coal fluidity and swelling.

To address these problems, attempts have been made to use the mathematics of percolation theory as an alternative to Monte Carlo calculations (6,23,24). Percolation theory gives closed-form solutions for a Bethe lattice. Keeping in mind that an actual coal network contains some different features from the Bethe lattice (e.g. the Bethe lattice has no loops), we made use of some basic concepts of percolation theory while we further modified the mathematics of this theory to describe vaporization processes in coal devolatilization.

One of the key parameters of percolation theory is the coordination number, $\sigma + 1$ which describes the possible number of bridge attachments per ring cluster (monomer). A linear chain has $\sigma + 1 = 2$, while a rectangular "fish net" has $\sigma + 1 = 4$. The higher the coordinator number, the more bridges must break to create network fragments. In attempting to apply percolation theory to the FG-DVC model (6), it became obvious that the single coordination number lattice used in most applications of percolation theory was not appropriate to describe coal network decomposition. It appears from solvent swelling data (25-29) and NMR data (30), that coal begins as a chain-like material with crosslinks every 2 to 8 ring clusters, i.e., $\sigma + 1$ between 2.2 and 2.5. So, its decomposition requires a low coordination number. However, crosslinking processes can occur at elevated temperature to increase the coordination number. Therefore, we extended the mathematics of percolation theory from a one-dimension probability computation into a two-dimensional probability computation to describe the coal network as a lattice with two bond types per cluster, i.e., two coordination numbers. This modified theory is referred to as the two- σ model (6).

Two important new features in our two- σ percolation theory are: (i) tar vaporization and (ii) molecular weight distribution of monomers. These features are basically treated the same way as in the original DVC model. The molecular weight of monomers is described by a probability distribution, which allows for the fact that monomers are made of various multi-ring structures. Tar molecules are removed out of the coal network using Suuberg's modified vaporization law. Molecular weight distributions of tar and char are kept track of during pyrolysis by a bookkeeping of the vaporization process in each mass bin. The percolation theory gives the mass fraction of all n-mers during pyrolysis. Combining this with a given molecular weight distribution of monomers, one can obtain the mass fraction of coal in each mass bin, which consists of two components: char and tar. Tar vaporization is computed for each mass bin. Tar in each mass bin monotonically increases and reduces the amount of char available for vaporization in the same bin until the char bin is emptied. Figure 9 shows the comparison of predicted tar yields between the Monte Carlo method and the modified percolation theory. Also, a two- σ prediction of the fluidity for the same coal is included in Fig. 3. The Monte Carlo and two- σ predictions agree reasonably well with each other and with the data.

CONCLUSIONS

This paper describes a number of improvements and extensions of the FG-DVC model of coal devolatilization.

- 1) Polymethylenes have now been included in the model. They account for part of the low temperature vaporization peak observed for some coals, and for the increase in the H/C ratio of coal tar observed for low rank coals.

- 2) A fluidity model has been added to the FG-DC model. The fluidity is dependent on the relative amounts of the liquid and solid, and on the fluidity of the liquid component. The fluidity of the liquid component depends on the average molecular weight of the liquid and on the temperature. The model accurately predicts the measured fluidities for the Argonne coals using rank dependent kinetics.
- 3) Rank dependent kinetics for tar formation, CO₂ formation and CH₄ formation have been obtained for the Argonne coals by fitting the fluidity data. These agree with rates obtain by fitting data from a TG-FTIR experiment at several heating rates and with the rates obtained by Burnham et al. (22) for the same set of coals.
- 4) The tar transport model used in the original FG-DVC model (i.e., the tars reach their equilibrium vapor pressure in the light gases and evolve with these gases as they are transported through the pores or by bubble transport) was examined by comparing the temperature and molecular weight predictions for tar evolution measured in a FIMS analysis. The original assumptions give reasonably good fits to the data if the Suuberg et al. vapor pressure correlation (5) is multiplied by ten.
- 5) A new two- σ percolation theory was developed with an approximation for tar evolution. The predictions of this model agree with the predictions using Monte Carlo statistics and with the data.

ACKNOWLEDGEMENT

The work was supported under Department of Energy, Morgantown Energy Technology Center Contract No. DE-AC21-86MC23075. Richard Johnson is the Project Manager.

REFERENCES

1. Solomon, P.R., Hamblen, D.G., Carangelo, R.M., Serio, M.A., and Deshpande, Energy & Fuel 2, 405, (1988).
2. Solomon, P.R., Serio, M.A., Deshpande, G.V., and Kroo, E., "Crosslinking Reactions During Coal Conversion", Energy & Fuels, accepted for publication (1990).
3. Solomon, P.R., Best, P.E., Yu, Z.Z., and Deshpande, G.V., ACS Div. of Fuel Chem. Preprints, 34, (3), 895, (1989).
4. Serio, M.A., Solomon, P.R., Yu, Z.Z., and Deshpande, G.V., "An Improved Model of Coal Devolatilization", presented at the Int. Conf. on Coal Sci., Japan, (1989), see also Serio, M.A., Solomon, P.R., Yu, Z.Z., and Basilakis, R., ACS Div. of Fuel Chem. Preprints, 34, (4), 1324, (1989).
5. Suuberg, E.M., Unger, P.E., and Lilly, W.D., Fuel, 64, 956, (2985).
6. Solomon, P.R., Best, P.E., Yu, Z.Z., and Deshpande, G.V., ACS Div. of Fuel Chem. Preprints, 34, (4), 1280, (1989).
7. Nelson, P.F., Fuel, 66, 1264, (1987).
8. Calkins, W.H., Hagaman, E., and Zeldes, H., Fuel, 63, 1113, (1984).
9. Calkins, W.H., Tyler, R.J., Fuel, 63, 1119, (1984).
10. Calkins, W.H., Fuel, 63, 1125, (1984).
11. Calkins, W.H., Hovsepian, B.K., Drykacz, G.R., Bloomquist, C.A.A., and Ruscic, L., Fuel, 63, 1226, (1984).
12. Freihaut, J.D., Proscia, W.M., and Seery, D.J., ACS Div. Fuel Chem. Preprints, 33, (2), 262, (1988).
13. Carangelo, R.M., Solomon, P.R., and Gerson, D.G., Fuel, 65, 960, (1987).
14. Whelan, J.K., Solomon, P.R., Deshpande, G.V., and Carangelo, R.M., Energy & Fuel, 2, 65, (1988).
15. Solomon, P.R., Serio, M.A., Carangelo, R.M., Basilakis, R., Gravel, D., Baillargeon, M., Baudais, F., and Vail, G., "Analysis of the Argonne Premium Coal Samples by TG-FTIR", Energy & Fuel, submitted for publication (1989).
16. Oxley, G.R. and Pitt, G.J., Fuel, 37, 19, (1958).
17. Fitzgerald, D., Fuel, 35, 178, (1956).
18. Van Krevelen, D.W., Coal, Elsevier, Amsterdam, (1961).
19. These data were provided by George Engelke of Commercial Testing and Engineering, Co.

20. Serio, M.A., Hamblen, D.G., Markham, J.R., Solomon, P.R., *Energy & Fuels*, **1**, 138, (1987).
21. Solomon, P.R., and Hamblen, D.G., "Pyrolysis," in Chemistry of Coal Conversion, Plenum Press, (R.H. Schlosberg, Ed.), New York, 1985, Chapter 5, p. 121.
22. Burnham, A.K., Oh, M.S., Crawford, R.W., and Samoun, A.M., *Energy & Fuel*, **3**, 42, (1989).
23. Niksa, S. and Kerstein, A.R., *Fuel*, **66**, 1389, (1987).
24. Grant, D.M., Pugmire, R.J., Fletcher, T.H., and Kerstein, A.R., *Energy & Fuels*, **3**, 175, (1989).
25. Green, T, Kovac, J, Brenner, D., and Larsen, J., in Coal Structure, (R.A. Myers, Ed.), Academic Press, NY, Chapter 6, p. 199, (1982).
26. Sanada, Y. and Honda, H., *Fuel*, **45**, 295, (1966).
27. Lucht, L.M. and Peppas, N.A., *Fuel*, **66**, 803, (1987).
28. Larsen, J.W. and Kovac, J., *ACS Symposium Series*, **71**, 36, (1978).
29. Lucht, L.M. and Peppas, N.A., *ACS Symposium Series*, **169**, 43, (1981).
30. Solum, M., Pugmire, R.J., and Grant, D.M., *Energy & Fuels*, **3**, 40, (1989).

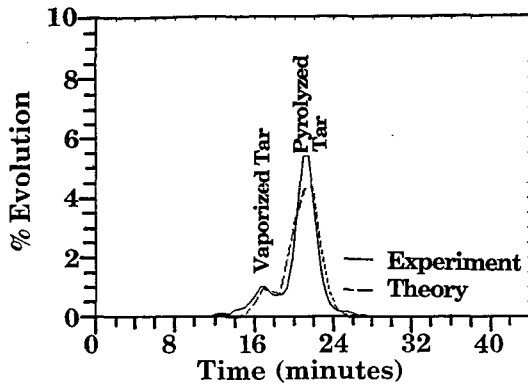


Figure 1. Comparison of FG-DVC Model Predictions for Tar Evolution Rate from Upper Freeport Coal with TG-FTIR Data.

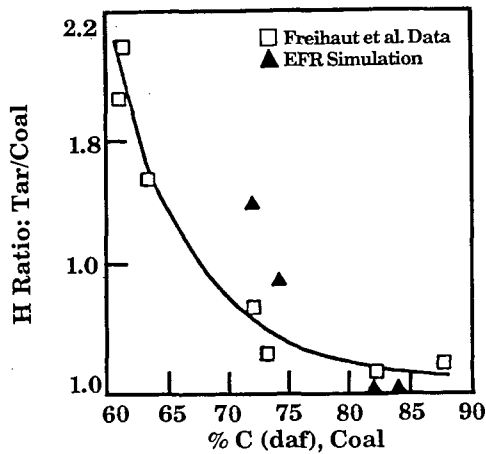


Figure 2. Ratio of % H in Tar to % H in Coal as a Function of Coal Rank. (from Freihaut et al. (12)).

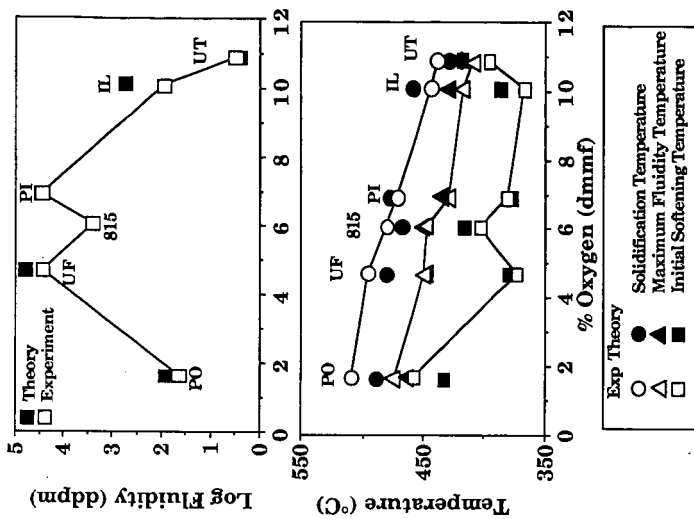


Figure 4. Fluidity Behavior as a Function of Coal Rank: Theory and Experiment. a) Maximum Fluidity Values and b) Fluidity Temperatures.

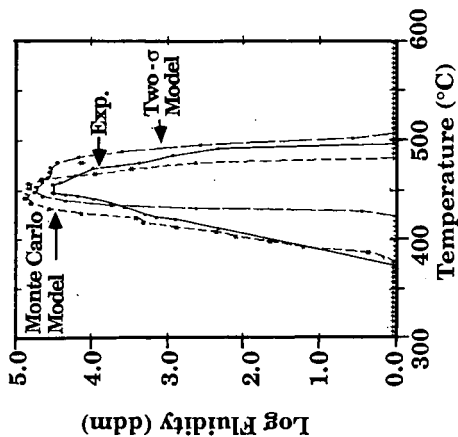


Figure 3. Fluidity of Upper Freeport Coal: Experiment (solid), Monte Carlo Theory (dashed) and Percolation Theory (dash-dot).

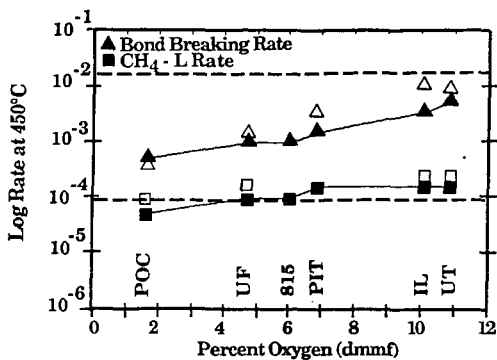


Figure 5. Rank Dependence of Kinetic Rates for Argonne Coals. Open Symbols: From Analysis of TG-FTIR Data at Four Heating Rates. Closed Symbols: From Fitting Fluidity Data at 3°C/min and TG-FTIR Data at 30°C/min. Dashed Lines: Rank Independent Rates used in Original FG-DVC Model.

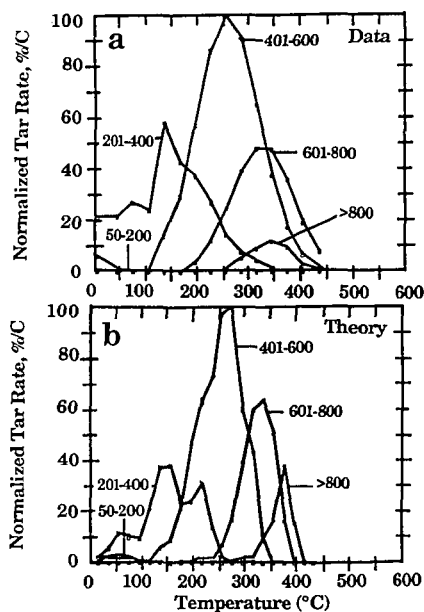


Figure 6. Comparison of a) FIMS Data and b) Theory for Pittsburgh No. 8 Coal Tar.

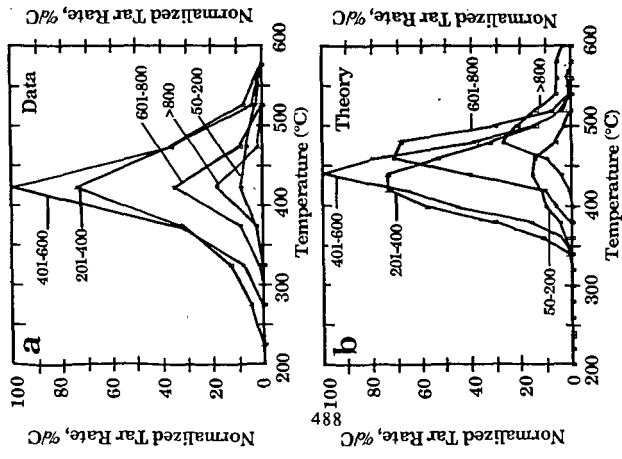


Figure 7. Comparison of a) FIMS Data and b) Theory for Normalized Tar Rate for Pittsburgh No. 8 Coal Pyrolyzed in the FIMS.

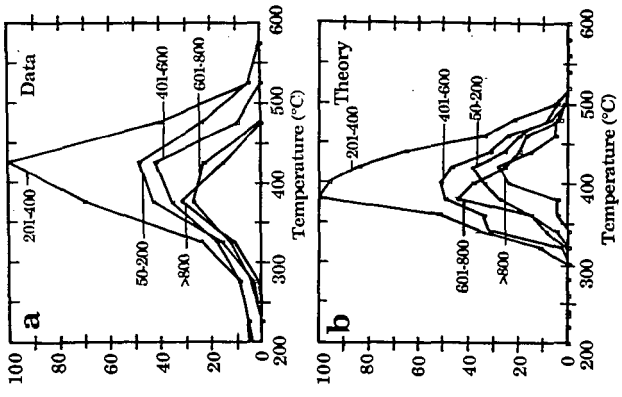


Figure 8. Comparison of a) Data and b) Theory for Normalized Tar Rate for Wyodak Coal Pyrolyzed in the FIMS.

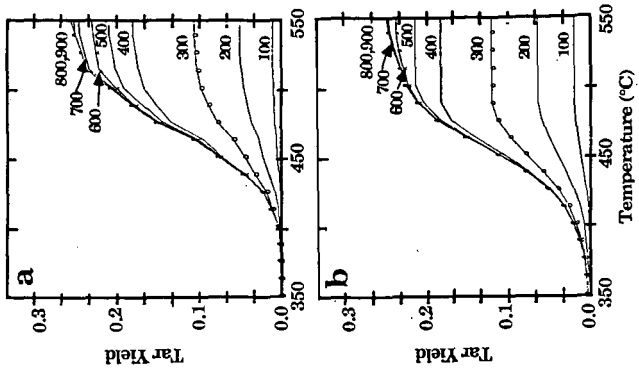


Figure 9. Comparison of Tar Molecular Weight Distribution Predicted with: a) Monte Carlo Method and b) Two- σ Percolation Theory.

MINERAL MATTER EFFECTS IN COAL PYROLYSIS

Insoo Bae, Majed Anani, Waleed Maswadh, Yongseung Yun, Henk Meuzelaar and Joel DuBow

Center for Micro Analysis and Reaction Chemistry, University of Utah
214 EMRL, Salt Lake City, Utah 84112

KEYWORDS: pyrolysis, coal, minerals

INTRODUCTION

Coal pyrolysis is a fundamental first step in combustion processes [1]. Yet coals exhibit a wide variation in pyrolysis behaviors. The origins of these wide variations are, for a given set of experimental conditions, both structural and compositional in nature. Because of its thermochemical and catalytic properties, mineral matter plays an important role in both the thermodynamics (product mixes, activation energies) and kinetics of coal pyrolysis [2]. The issue is further complicated by the manner in which mineral matter is distributed in various coals. While many classifications are possible, grouping into three classes is most common [3]. These classes are: (1) discrete minerals such as clays, oxides (basic and acidic) and sulfides; (2) organometallic matter such as ion-exchangeable cations; and (3) dispersed trace elements and compounds. A considerable body of research exists for studying equilibrium and non-equilibrium effects of the various forms of coal minerals on coal combustion [4,5,6].

In the present paper the mineral matter effects on coal pyrolysis are being analyzed using an approach whereby observable spectroscopic (TG/MS) differences in the pyrolytic decomposition between fresh coal and demineralized coal are reconstructed from the sum of mineral matter effects on pyrolysis arising from adding back, singly and in pairs, individual minerals in various forms.

EXPERIMENTAL TECHNIQUE

A low rank coal, Beulah Zap lignite was chosen because of its readily exchangeable cations, the strategic and technological importance of the huge Northern Great Plains lignite resource, and its availability as a standard reference coal through the Argonne National Laboratory Premium Coal Sample Program (ANL-PCSP).

Prior to sample preparation, coal is freezer stored under Ar or N₂ at -30 to -90 C so that oxidation is prevented. A standard HCl/HF acid wash is used to demineralize the coal. This has been shown not to alter coal structure [6], but does influence the number of reactive sites and surface reactivity in the coal [8,9].

Subsequently, cations and/or minerals are added back into the coal following demineralization. The cations are added using titration techniques and the sulfide or oxide minerals, as well as the clays, added by physical mixing. The titration results agree within +/- 10% of ICP/AES (Inductively Coupled Plasma/Atomic Emission Spectroscopy) determinations. Figure 1 shows the comparison of the titration ion concentration with the ICP/AES measurements.

Following sample preparation, pyrolytic decomposition is studied. Thermochemical kinetics are obtained using a home-built thermogravimetry/mass spectrometry (TG/MS) system [10] in conjunction

with PAS (photoacoustic spectroscopy) using an MTEC model 200 PAS cell and Perkin Elmer Model X1760 FTIR system. The yield of char or ash is quantified using TGA and mineral concentrations are quantified using ICP/AES. Data for each run are replicated three times, and a minimum of three heating rates per sample composition are run in order to evaluate the kinetic parameters using one of three statistical kinetic programs.

EXPERIMENTAL RESULTS

Sample Preparation-- Figure 2 demonstrates the effectiveness of the concentrated HF/HCl demineralization procedure. The ICP/AES data show that 95% of the mineral matter was removed. Furthermore, TG/MS data, as exemplified in Figures 3a and 3b, indicate that major structural transformations do not occur as a result of demineralization.

Minerals were subsequently added to the demineralized coal by physical mixing or by ion exchange titration. Figure 4 shows FTIR data including the computed difference between fresh (Figure 4a) coal and demineralized (Figure 4b) coal FTIR spectra. Figure 4c shows the difference between FTIR spectra for fresh Beulah Zap coal and demineralized Beulah Zap. The peaks at 1090 cm^{-1} are particularly significant for cations and mineral phases. Note the strong similarities between the calculated difference spectrum in Figure 4c and the measured spectrum of ash obtained by low temperature ashing (Figure 4c). The effect of adding calcium is also given. The peaks for hydrogen replacement of cations and for the existence of mineral phases are consistent with known ion exchange and mineral substitution mechanisms.

Coal Pyrolysis - The effects of demineralization and of adding 2.6% Fe to demineralized Beulah Zap on specific products of devolatilization are shown in selected, time- and temperature-resolved mass spectral data in Figure 3.

Figure 3a-d shows the influence of demineralization (followed by adding iron chloride to demineralized coal) upon the DTG curve, the total ion count signal and the time (or temperature)-resolved ion profiles for H_2^+ (m/z 2), CO^+ (m/z 28), and H_2O^+ (m/z 18). The main features of the DTG profiles are replicated in the total ion count profiles. The mass spectral profiles for fresh and demineralized coal exhibit peak shifts in both temperature and amplitude. For iron, the concurrent sharp fall off of H_2O accompanied by a sharp rise in H_2 (which is doubly activated) and CO is strongly suggestive of a water-gas-shift reaction. Moreover, the activation energies, based on first order kinetics, are similar for H_2 and CO . Both calcium and iron affect the hydrogen generation kinetics.

Kinetics - A number of kinetic parameter-fitting models were evaluated for devolatilization kinetic parameter determination. The techniques of Yun (1989) and Burnham (1989) [11,12] are specifically focussed on distributed activation energy models. However, not all the reactions are necessarily uncoupled parallel first order reactions. The apparent activation energies and reaction order may be estimated from leading edge or TG/MS line profiles. Table 1 shows the computed activation energies for H_2 and CO . The hydrogen generation curve may arise from a number of possible mechanisms. The experimental data for DMBZ+ 2.6% FeCl_3 are indicative of two distinct reactions. The apparent activation energy of 42.2 K cal/mole is apparently increased by the contribution of lower temperature reactions (water-gas-shift and main pyrolysis reaction).

The existence of catalytic effects of mineral matter is reinforced by the thermochemical kinetic data enumerated in Table II. The fresh Beulah Zap coal activation energy is the highest and hence pyrolysis proceeds at the fastest rate. The lowest activation energy is for demineralized Beulah Zap

coal, while the activation energies for demineralized Beulah Zap samples with added iron and calcium lie in between.

CONCLUSIONS

Marked effects of iron and calcium cation content on the hydrogen, water, and carbon monoxide generation rates during pyrolysis were observed. In addition, the potential for PAS-FTIR spectroscopy in quantitative applications to coal spectra was demonstrated on fresh demineralized and remineralized coal. Demineralization and selected remineralization affect the rate of gas evolution in general and of hydrogen and carbon monoxide in particular. This is in good agreement with published literature data [13,14,15].

ACKNOWLEDGEMENTS

This work was sponsored by the Advanced Combustion Engineering Research Center. Funds for this Center are received from the National Science Foundation, the State of Utah, 23 industrial participants and the U.S. Department of Energy.

REFERENCES

1. Howard, J.B., "Fundamentals of Coal Pyrolysis and Hydrolysis," pp. 665-784, Chemistry of Coal Utilization, Elliott, M.A., (ed.), Wiley-Interscience, New York, 1981.
2. Gavalas, G., Coal Pyrolysis, Elsevier Publ. Co., New York, 1984.
3. Morgan, B.A., and Scaroni, A.W., "Cation Effects During Lignite Pyrolysis and Combustion," pp. 255-266, The Chemistry of Low Rank Coals, American Chemical Society, Washington, D.C., 1984.
4. Badin, E.J., Coal Combustion Chemistry Correlation Aspects, pp. 40-45, Elsevier, Amsterdam, 1984.
5. Lahaye, J., and Prado, G., "Porous Morphology of Coal: Its Transformation During Pyrolysis," pp. 159-177, Fundamentals of the Physical-Chemistry of Pulverized Coal Combustion, Martinus Nijhoff Publishers, Dordrecht, 1987.
6. Vorres, K., Mineral Matter and Ash in Coal, ACS Symposium Series, 1986.
7. Boni, A.A., "Transformation of Inorganic Coal Constituents in Combustion Systems," DE-AC22-86PC90751, 1989.
8. Jenkins, R.G., Walker, P.L., "Analysis of Mineral Matter in Coal," in Analytical Methods for Coal and Coal Products, Chapter 26, Academic Press, 1978, pp. 265-292.
9. Franklin, H.D., Cosway, R.G., Peters, W.A., and Howard, J.B., "Effects of Cations on the Rapid Pyrolysis of a Wyodak Subbituminous Coal," Ind. Eng. Chem. Process Des. Dev., 22:39-42, 1983.

10. Yun, Y., Meuzelaar, H.L.C., "Simultaneous Thermogravimetric and Mass Spectrometric Observations on Vacuum Pyrolysis of Argonne PCSP Coals," ACS Preprints, Div. Fuel Chem., Vol. 33(3), 1988, pp. 75-84.
11. Yun, Y., and Maswadeh, W., Meuzelaar, H.L.C., Simmleit, N., Schulten, H.R., "Estimation of Coal Devolatilization Modeling Parameters from Thermogravimetric and Time-Resolved Soft Ionization Mass Spectrometric Data," ACS Preprints, Div. Fuel Chem., Vol. 34(4), 1989, pp. 1308-1316.
12. Burnham, A.K., oh, M.S., and Crawford, R.W., "Pyrolysis of Argonne Premium Coals: Activation Energy Distributions and Related Chemistry," Energy and Fuels, 3(1): 42-55, 1989.
13. Scaroni, A.W., Walker, P.L., and Jenkins, R.G., "Effect of Surfaces on the Yield of Volatiles from Coal," Fuel, 60:558-560, 1981.
14. Yamashita, H., Ohtsuka, Y., Yoshida, S., and Tomita, A., "Local Structures of Metals Dispersed on Coal 1," Energy and Fuels, 3(6):686-692, 1989.
15. Morgan, M.E., and Jenkins, R.G., "Role of Exchangeable Cations in the Rapid Pyrolysis of Lignites," pp. 213-226, The Chemistry of Low Rank Coals, American Chemical Society, Washington, D.C., 1984.

TABLE I
ACTIVATION ENERGIES FOR HYDROGEN AND CO

Coal Sample*	Mass Peak	Activation Energy (kcal/mol)	Observed Temp. Range (K)
FRBZ	m/z 2 (H ₂ +)	36.8	800-1200
	m/z 28 (CO+)	22.7	800-1200
DMBZ + 2.6% Fe	m/z 2 (H ₂ +)	42.2	800-900
	m/z 28 (CO+)	35.2	800-1200

* FRBZ = Fresh Beulah Zap
DMBZ = Demineralized Beulah Zap

TABLE II
ACTIVATION ENERGIES BASED ON TG WEIGHT LOSS DATA

Coal Sample*	E _a (kJ/mol)	Chosen % Conversion	Heating Rate Used
FRBZ	213 ± 43.68	30, 32, 34, 36, 38, 40	5, 10, 25, 50
DMBZ	102.79 ± 32.72	15, 18, 21, 24	5, 10, 25
DMBZ + Fe	131.94 ± 51.40	30, 32, 34, 36, 38	10, 25, 50
DMBZ + Ca	144.44 ± 40.67	30, 32, 34, 36, 38, 40	10, 25, 50

* see Table I

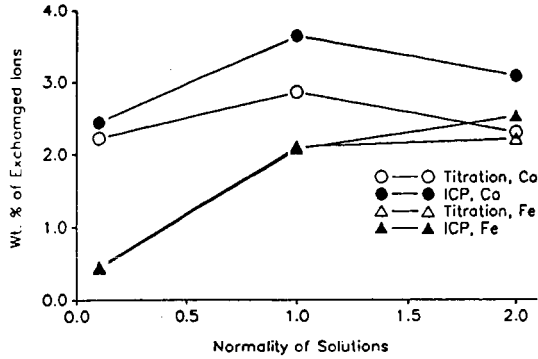


Figure 1. Ion exchange was accomplished via titration and verified by ICP/AES. The iron substitution data are nearly identical, indicating a more effective exchange than for calcium. The concentration in the coal tends to saturate above 1N solutions.

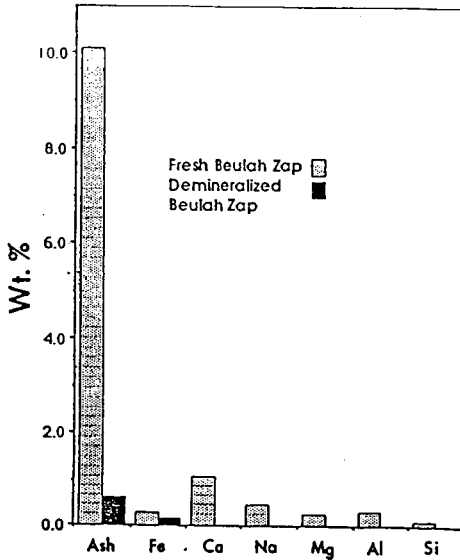
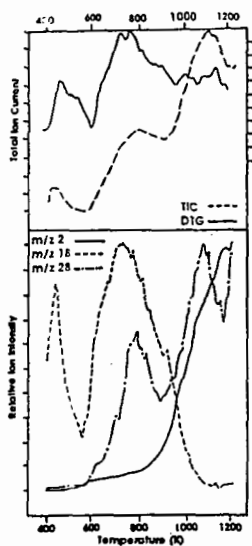
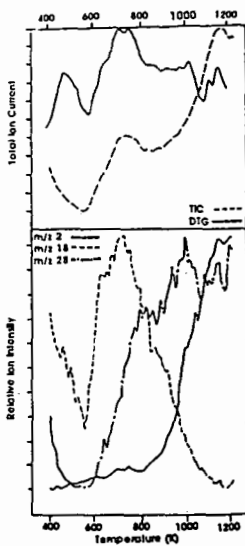


Figure 2. ICP-AES data for fresh and demineralized Beulah Zap coal. While the efficiency for mineral removal varies by element, the demineralization is seen to remove about 95 percent of the total mineral matter.

a. Fresh Beulah Zap



b. Demineralized Beulah Zap



c. as b + 2.6% Fe

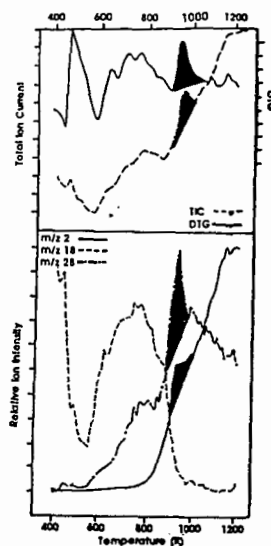


Figure 3. Selected thermogravimetric weight loss, total ion count and mass spectral profiles for H_2O , CO and H_2 is demineralized and remineralized Beulah Zap coal. Of note are the duplication of the main DTG features in the total ion count and the evidence in Figure 4c (see shaded areas) of water-gas-shift reactions (falling water concentration with concurrently rising hydrogen and CO concentrations). The iron cations shift the hydrogen profile to lower temperatures with accompanying rapid rise in CO . The activation energies for H_2 (m/z 2) in Table I are indicative of two interacting reactions for hydrogen generation, e.g., water-gas-shift and crosslinking.

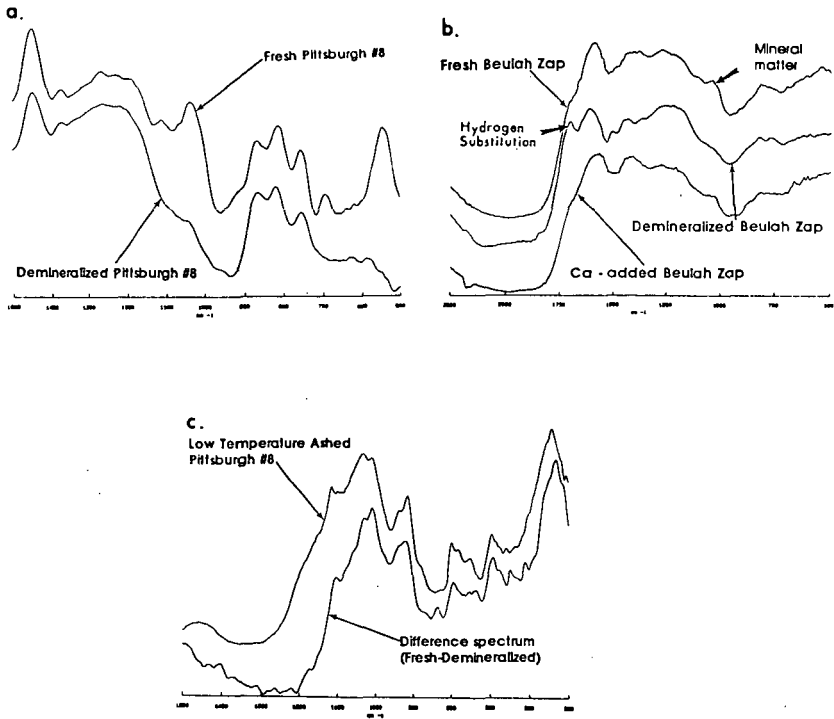


Figure 4. Photoacoustic FTIR spectra for fresh and demineralized Pittsburgh #8 and Beulah Zap coals. Of particular note in Figure 4a and c are the strong similarities between the computer difference spectra (between fresh and demineralized coal) and the ash spectra. Figure 4b shows the verification of calcium ion exchange in Beulah Zap coal through the FTIR spectral shifts at 1690 cm^{-1} and 1050 cm^{-1} between fresh, demineralized and Ca-added coals.

ANOMALOUS SIDE CHAIN CLEAVAGE IN ALKYLAROMATIC PYROLYSIS

H. Freund, M. G. Maturro, W.N. Olmstead, R.P. Reynolds, and T.H. Upton
Corporate Research
Exxon Research and Engineering Co.
Route 22 East
Annandale, NJ 08801

Keywords: Alkylpyrene thermal chemistry, Side chain cleavage, Radical hydrogen transfer.

INTRODUCTION

In reactions of hydrocarbons, alkylaromatic side chain cleavage occurs as the result of thermal or acid catalyzed cracking chemistry. In general, acid catalysis leads to direct bond cleavage at the aromatic ring whereas thermally promoted bond breaking gives primarily substituted aromatics.¹ The formation of a core aromatic by a thermal process is expected only at higher temperatures and in low yield due to the need for hydrogen atoms.

The thermal chemistry of simple alkyl substituted aromatics has been extensively studied both experimentally² and mechanistically³ over a wide range of temperatures in the gas and liquid phase. Selectivity and conversion can generally be explained by the classical Rice-Hertzfeld chain mechanism,⁴ involving initiation, chain propagation and termination steps.

Typically, thermal cleavage of an alkyl group at the ring for most systems studied (1 and 2 ring alkylaromatics) is observed only at relatively high temperature. It occurs by ipso hydrogen atom attack followed by cleavage and rearomatization by loss of the alkyl side chain.⁵

Recently, for the alkylpyrene system, extensive direct side chain cleavage has been observed for liquid phase, low temperature (375-425°C) pyrolysis (43% yield of pyrene at 400°C and 180 min.).⁶ Pyrene formation was reported to be the result of autocatalysis. This yield of core aromatic is much greater than that found for single ring aromatics.² Detailed mechanistic interpretation of this work is obscured by the high levels of conversion and formation of higher molecular weight residues.

In this paper, we wish to report the results of a combined theoretical and experimental study which we believe does provide experimental confirmation of a direct cleavage path. In support of this conclusion, we present an analysis of the possible reaction pathways.

EXPERIMENTAL SECTION

The model compound used in the pyrolysis studies, 1,20-di(1-pyrenyl)icosane (1) was obtained from Molecular Probes Inc., Eugene, Oregon and used without further purification. The material was 99 % pure by high temperature gc.

Nuclear Magnetic Resonance spectra were recorded using a Brüker AM-360. Peak positions were referenced to tetramethylsilane (TMS) and all spectra were run in CDCl₃. Products were analyzed by gc using either a HP 5890 equipped with an FID detector (column 30M x 0.32mm I.D. SPB-5, cross-linked methyl silicone, 0.25µ) operated in the splitless mode or a Carlo Erba HT SIM-DIST (high temperature simulated distillation) GC. Mass spectral analyses were conducted using an HP5995 GC/MS with RTE-6 Data Station equipped with a column identical to that described above for the HP5890.

A Perkin Elmer TGS-2 Thermogravimetric System was modified and operated to achieve heatup rates up to 20 times faster than it was designed for. The reactor and balance mechanism were enclosed and continuously purged with helium. The TGA thermocouple was calibrated using high temperature Curie Point metals as recommended by Perkin Elmer.

Flash Pyrolysis studies were carried out using a commercial pyroprobe instrument (Chemical Data Systems, Inc. CDS 122 Pyroprobe) equipped with an electrically heated platinum coil on the end of an

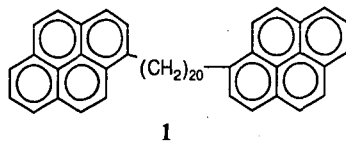
insulated probe. In a typical experiment, the nonvolatile model compound of interest was coated on the wire by placing a small amount of the organic material onto the coil and then heating until the material melts and formed a thin film on the surface. The probe was then fitted with a glass tube sealed at one end, and the pyrolysis chamber was purged with helium. The coil was then rapidly heated to temperature (600 to 1000°C max.) at the maximum rate possible (nominally 20,000 °C per sec) and maintained at temperature for the desired reaction time. Products collected on the inside surface of the air cooled tube and were washed down the tube with solvent and analyzed by gc, gc/ms, and ¹H NMR spectroscopy.

A detailed chemical kinetic model for the pyrolysis of **1** was constructed using an abbreviated set of reactions from the modeling of butylbenzene.³ The thermochemistry was changed to reflect the increased stability of the 4-ring benzylic like radical relative to the one ring case. Stein and Golden estimate this to be 8 kcal/mole.⁷

RESULTS AND DISCUSSION

Pyrolysis Experiments

We have conducted pyrolyses using open reactor configurations and flash pyrolysis methods. The model used was 1,20-di(1-pyrenyl)eicosane (**1**) (bp. ~620°C, estimated from gc simulated distillation).



When **1** was pyrolyzed in an open reactor (TGA) at 425 and 512°C, the sample weight loss was monitored as a function of time. The products were collected and analyzed by high temperature GC. Liquid product recovery was nearly quantitative (99%) plus a 3% yield of a nonvolatile residue (total mass recovery 102 %) for the 425°C sample. For the 512°C sample, liquid and residue yield were 94 and 2% respectively (total mass recovery 96%).

GC results show some starting material in the volatile liquids (32 % at 427 °C and 9 % at 512°C) and the formation of a substantial amount of pyrene and its paired pyrolysis product, 1-eicosylpyrene as well as the usual series of paired alkyl and terminal alkenylaromatics. This confirms the importance of an anomalous direct side chain cleavage pathway in alkylpyrene pyrolysis. It also indicates the extent of volatilization of **1** under the TGA experimental conditions.

In figures 1a and b, a schematic representation of the product selectivity data is given for the 427 and 512 °C runs. The plots clearly show the general pairing of products when an internal carbon-carbon bond is cleaved. Comparison of the plots demonstrates the suppression of pyrene production at high temperature. This is consistent with the sealed tube data in reference 6. Table I quantifies these trends for the alkylpyrenes, includes flash pyrolysis data for **1** at 575°C, and includes product selectivities for butylbenzene at 505°C for comparison.

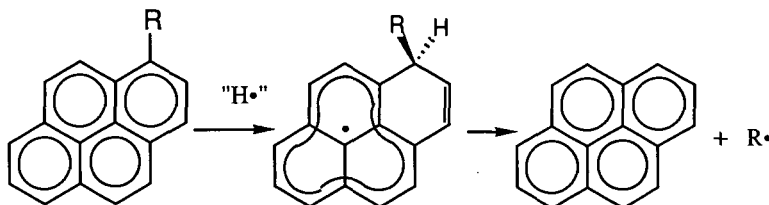
The proton NMR spectrum for the products derived from flash pyrolysis at 425°C is shown in figure 2 with an enlargement of the olefin region. The four multiplets on the right of this region are unambiguously assigned to the terminal hydrogens of vinylpyrene and the olefinic hydrogens of the series of terminal olefins (chain length greater than C₂) substituted on pyrene.⁸ The downfield multiplet is assigned to the beta hydrogen of an alkyl substituted vinylpyrene (see fig. 2b). Its chemical shift and coupling pattern are consistent with the trans isomer. Figure 2b shows a comparison of the experimentally observed adsorption and a spectral simulation.⁹ Using standard literature coupling constants,¹⁰ excellent agreement is obtained.

Formation of the internal olefin discussed above provides a candidate for the missing source of hydrogen needed for side chain cleavage. Confirming support for this hypothesis was obtained by tracking the formation of this species relative to pyrene at different temperatures. The ratios for pyrene to vinylpyrene and internal olefin to vinylpyrene are 0.46 and 0.41 (575°C max.) and 0.24 and 0.21 (800°C max.)

respectively.¹¹ These values clearly show that formation of the internal olefin is coupled to pyrene formation.

Mechanistic Interpretations

In the general case, three mechanistic possibilities exist for the conversion of an alkylpyrene to pyrene and an alkane. They are distinguished by the following elementary reaction features: 1) ipso hydrogen atom addition, 2) bimolecular radical hydrogen transfer, RHT (transfer of hydrogen from a location beta or, in the general case, distant from the site of highest spin density at alternate carbons),^{12,13} and 3) a multistep path with internal hydrogen transfer. All are assumed to involve the intermediacy of an adduct formed from the addition of a hydrogen atom to position 1 of the 1-substituted pyrene. The resulting species from this addition is a very stable polycyclic aromatic π -radical and is formally a vinyl substituted perinaphthyl radical (2). It is also expected that this intermediate will fragment rapidly to give the parent pyrene and an alkyl radical. The critical mechanistic steps concern the formation of 2.



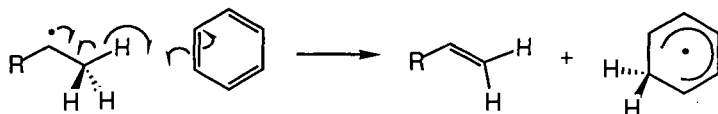
2

Ipsa Hydrogen Atom Addition

The production of pyrene and n-C₂₀-pyrene decrease with increasing temperature. Previous experimental and modeling results on butylbenzene show an increase in benzene production by ipso hydrogen atom addition with increasing temperature. Kinetic modeling results in this work also show that an ipso hydrogen atom addition would yield an increase in side chain cleavage with increasing temperature. Since the experimental results are opposite this trend, we believe that free hydrogen atoms are not the primary cause of the cleavage.

Radical Hydrogen Transfer (RHT)

Examination of the radical hydrogen transfer pathway from a thermochemical kinetic perspective requires a knowledge of the intrinsic reaction barriers and the heats of formation of the intermediates. For the proposed direct radical hydrogen transfer mechanism, little information exists concerning the barrier heights for this process.

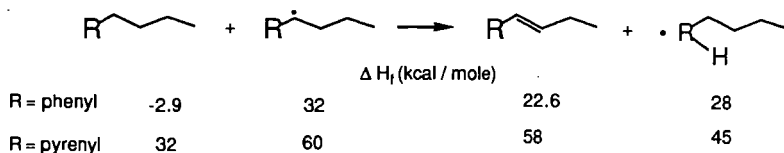


An estimate of the barrier for radical hydrogen atom transfer (RHT) can be calculated from literature rate constants for a nearly degenerate case ($\Delta H = 0$) involving transfer of hydrogen from a 2-ethyl-9-hydroanthryl to anthracene.¹⁴ Using a typical bimolecular pre-exponential factor, an E_a value of 18 kcal/mol is obtained.

From the above discussion, a key piece of information required to assess the viability of RHT as a mechanistic alternative is a quantitative estimate of the pyrene-derived vinylperinaphthyl radical stabilization energy. Estimates of hydrogen atom addition heats to a series of polycyclic aromatic systems have been reported. Unfortunately, large disagreement exists for the pyrenyl and phenanthryl ring systems. For perinaphthyl radical, estimates of resonance stabilization range from 22 to 47 kcal/mole

depending on the form of resonance-structure theory used.¹⁵ To resolve this critical issue for our own work we have developed a linear free energy correlation using the reliable heats of hydrogen atom addition^{15,16} and the reported rates of methyl¹⁷ and trichloromethyl¹⁸ radical addition to a series of polycyclic aromatic hydrocarbons. Given an appropriate reaction heat, a reliable estimate of perinaphthyl radical stabilization energy can be computed from known or easily estimated quantities. The vinyl perinaphthyl radical stabilization energy is estimated to be 46.7 kcal/mole which is close to the high range value estimated by Stein¹⁵ ($\Delta H_1(\text{perinaphthyl}) \sim 32\text{-}47$ kcal/mole) using Herndon's methods¹⁶ for perinaphthyl itself.

For simplicity the butylpyrene system is used in all thermochemical estimates instead of 1. Given a stabilization energy of 47 kcal/mole for the vinyl-perinaphthyl system, a reaction heat can be calculated for bimolecular radical hydrogen transfer for the pyrenyl and phenyl systems.



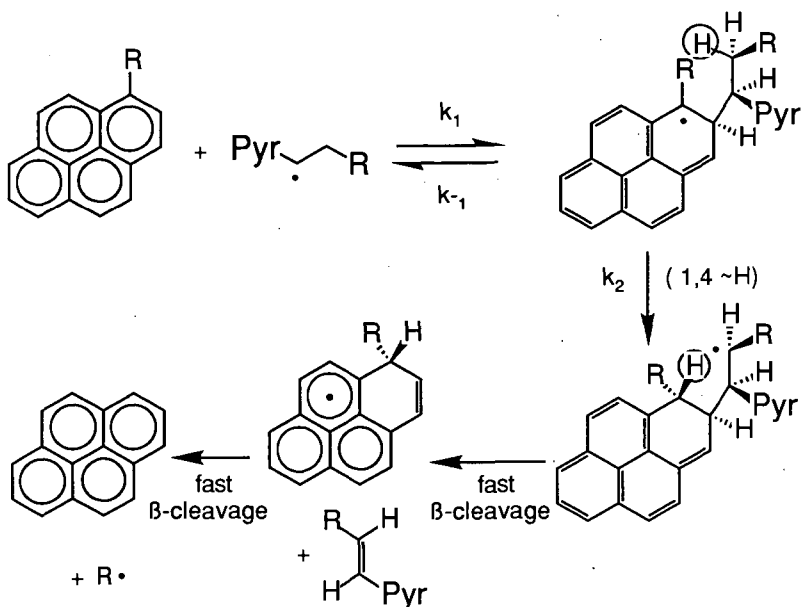
An enthalpy of 21 kcal/mole is obtained for the butylbenzene system while the overall reaction with butylpyrene gives a ΔH_{rxn} of 11 kcal/mole. In both cases the reaction gives a delocalized radical and an internal olefin conjugated to an aromatic ring. Summing the barrier estimate for remote hydrogen transfer (RHT) calculated from Stein's work ($E_a = 18$ kcal/mole) and all of the reaction enthalpy for the butylpyrene case gives a total barrier of 29 kcal/mole for this elementary step (RHT). This value would be an upper limit since all of reaction enthalpy would not be felt at the transition state. To put this value in perspective, note that the typical activation energies for thermoneutral hydrogen transfer are in the range of 10-13 kcal/mole. The reaction transferring a hydrogen atom from the highly stabilized benzylic radical in a pyrene system to form a secondary unstabilized radical is about 20 kcal/mole endothermic, leading to an activation energy in the range of 30-33 kcal/mole. Hence a process with a 29 kcal/mole activation energy for this radical hydrogen transfer should be quite competitive with conventional hydrogen transfer. Indeed, these values would suggest that at higher temperatures, if hydrogen transfer were rate limiting, conventional hydrogen transfer would begin to win out over this new reaction, leading to the observed temperature dependence of the selectivity.

To derive an estimate of the RHT barrier from the TGA data of the pyrolysis of 1, the existing model for butylbenzene pyrolysis was modified. Changes were made to make the model appropriate for butylpyrene (adjustment for increased radical stabilization by pyrene) and the inclusion of RHT hydrogen transfer step (see experimental section). The kinetic parameters for this reaction were adjusted to match the experimental measurements. This yielded a barrier of 25 kcal/mole [$k = 3.5 \times 10^{11} e^{(-25000/RT)}$ cc/mole-sec] which is close to the above estimated value of 29 kcal/mole.

For the single ring aromatic case, the large reaction enthalpy and intrinsic barrier (21 + 18 = 39 kcal/mole) suggests that remote hydrogen transfer will not occur in that system and explains why little cleavage at the ring is observed experimentally.

Multistep Pathway

The third mechanistic possibility for side chain cleavage at the pyrene ring involves a sequence of elementary steps: addition, intramolecular hydrogen transfer and cleavage to products. The scheme shown below details these steps for alkyipyrene side chain cleavage.



We estimate that the reaction enthalpy for addition and for the subsequent hydrogen transfer to be quite endothermic (~ 24 and 14 kcal/mole, respectively). Using a steady state analysis of the initial addition adduct and typical intrinsic barriers with these reaction enthalpies leads to a product production rate which is many orders of magnitude less than the observed rate constant for pyrene formation extracted from kinetic modeling. Hence, no multistep mechanism that we can envision competes with the remote hydrogen transfer pathway.

CONCLUSION

From our experimental work and modeling, we conclude that alkylpyrene side chain cleavage at the aromatic ring is unusual in two ways: First, it involves the specific structure of the pyrene system in that ipso addition of a radical generates a highly stable vinyl perinaphthyl radical and second, the critical, perinaphthyl like, intermediate is formed by a remote hydrogen transfer reaction. We estimated the heat of formation of the critical intermediate described above, and this supports a perinaphthyl radical stability of 47 kcal/mole, which is at the high end of literature values.

Product studies have revealed the formation of an internal olefin conjugated to pyrene during pyrolysis of model alkylpyrene which is produced in concert with pyrene. This provides confirming evidence for the source of hydrogen needed to effect bond cleavage. This information plus thermochemical analysis limits the mechanistic possibilities to a process that must involve direct bimolecular radical hydrogen transfer.

REFERENCES

1. Hansford, R.C. in Farkas, A. Ed., *Physical Chemistry of Hydrocarbons*; Academic Press: New York, 1953, 224-226.
2. a) Rebick, C. in W.A. Pryor, Ed., *Frontiers of Free Radical Chemistry*; Academic Press: New York, 1980, 117-137.; b) Savage, P.E.; Klein, M.T. *Ind. Eng. Chem. Res.* **1987**, *26*, 374 and *ibid.* **1987**, *26*, 488.

3. Freund, H.; Olmstead, W.N. *Int. J. Chem. Kinetics* **1989**, *21*, 561-574.
4. Kossiakoff, A.; Rice, F.O. *J. Am. Chem. Soc.* **1943**, *65*, 590.
5. Robaugh, D.; Tsang, W. *J. Phys. Chem.* **1986**, *90*, 4159.
6. Savage, P.E.; Jacobs, G.E.; Javanmardian, M. *Ind. Eng. Chem. Res.* **1989**, *28*, 647.
7. Stein, S. E.; Golden, D.M. *J. Org. Chem.* **1977**, *42*, 839-841.
8. ¹H NMR: Vinylpyrene terminal olefins (trans H, 5.98 ppm, J_{trans} = 17.4 Hz, J_{gem} = 1.2 Hz; cis H, 5.60 ppm, J_{cis} = 11 Hz, J_{gem} = 1.2 Hz); aliphatic chain olefins (terminal H's, 5.02-4.87 ppm, dd with allylic coupling, non terminal H, 5.79 ppm, multiplet).
9. Brüker spin system simulation software "PANIC", Parameter Adjustment in NMR by Iterative Calculation, 1985 version.
10. Typical coupling values were used in the simulation and gave peak positions and intensities nearly identical with the observed pattern; For the beta vinyl hydrogen in the internal olefin, J_{1,2}(trans olefinic coupling) = 15 Hz, J_{2,3}(olefinic to CH₂) = 5.8 Hz = J_{2,4}; Gorden, A.J., Ford, R. A. "The Chemist's Companion"; John Wiley & Sons; New York, 1972, 269.
11. The pyrene to vinylpyrene ratio was obtained by gas chromatographic analysis while the internal olefin to vinylpyrene ratio was obtained by integration of the olefinic region of the ¹H NMR spectrum (see figure 2).
12. McMillen, D.F.; Malhotra, R.; Chang, S.-J.; Ogier, W.C.; Nigenda, S.E.; Fleming, R.H. *Fuel* **1987**, *66*, 1611-1620.
13. Metzger, J.D. *Angew. Chem. Inter. Ed. Engl.* **1986**, *25*, 80.
14. Billmers, R.; Griffith, L. L.; Stein, S.E. *J. Phys. Chem.* **1986**, *90*, 517.
15. Stein, S. E. in R.H. Schlosberg, Ed., *The Chemistry of Coal Conversion*; Plenum Press: New York, **1985**, 13-44.
16. Hemdon, W.C. *J. Org. Chem.* **1981**, *46*, 2119.
17. Levy, M.; Szwarc, M. *J. Am. Chem. Soc.* **1955**, *77*, 1949.
18. Kooymann, E. C.; Farenhorst, E. *Trans. Faraday Soc.* **1953**, *49*, 58.

Figure 1a: Product Selectivities at 427°C Pyrolysis of 1

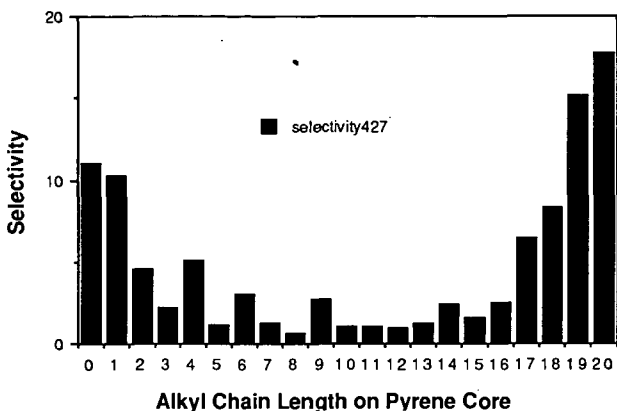


Figure 1b: Product Selectivities at 512°C Pyrolysis of 1

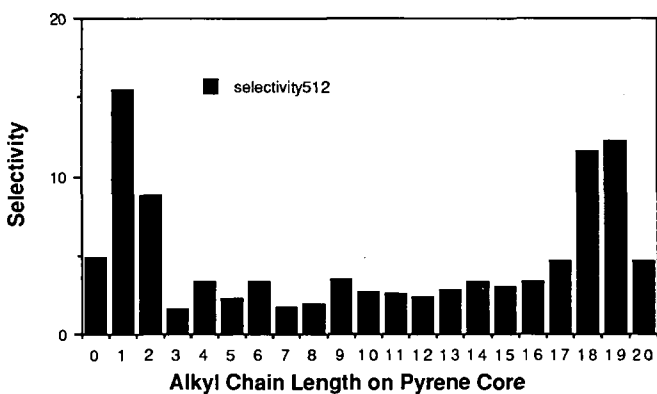


Figure 2a: ^1H NMR Spectrum (360 MHz) of Flash Pyrolysis (575°C max.) with Expansion and Blow-up of Olefinic Region.

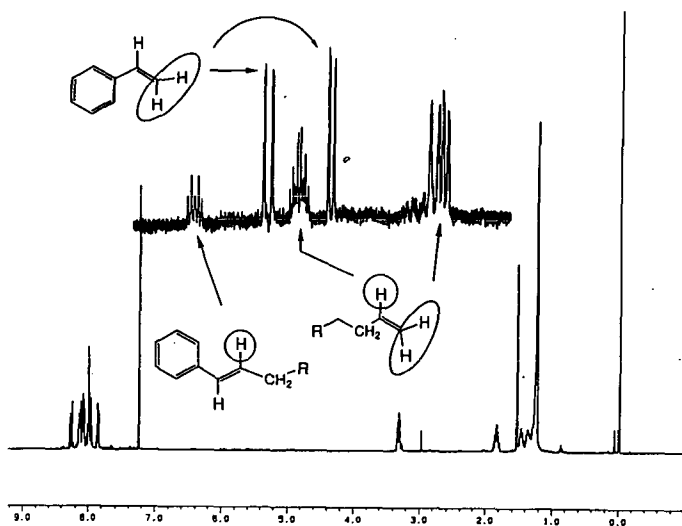


Figure 2b: Comparison of Measured and Simulated Proton NMR Spectrum of H_2 in the Internal Olefin Product.

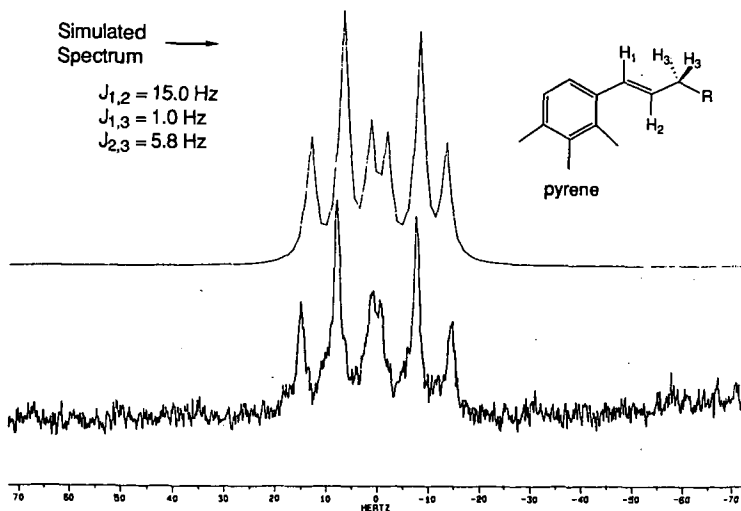


Table 1: Product Selectivities For Sealed Tubes (Savage et al.), OpenReactor (TGA), and Pt Wire (Flash Pyrolysis) Relative to Methylpyrene. Single Ring Data is for Butylbenzene.

	Savage et al.		TGA		Pt Wire	Single Ring Gas Phase
Pyrene	4.3	2.7	1.1	0.32	0.19	0.05
Methylpyrene	1.0	1.0	1.0	1.0	1.0	1.0
C2-pyrene	0.35	0.55	0.44	0.57	0.54	2.2
Temp. (°C)	375	425	425	510	575	505
Citation	ref. 6		this work		this work	ref. 2a

PYROLYSIS OF PLASTIC COALS: PORE STRUCTURE DEVELOPMENT AND CHAR REACTIVITY

Andreas Matzakos and Kyriacos Zygorakis
Department of Chemical Engineering
Rice University
Houston, Texas 77251-1892

Keywords: Coal pyrolysis, macropore structure of chars, char reactivity in oxygen.

INTRODUCTION

Complex morphological transformations accompany the chemical reactions occurring during the pyrolysis of coals. The structural changes are particularly evident during the pyrolysis of plastic coals. Such coals soften as they are heated up, and the evolving volatile gases form bubbles that swell the coal particles and lead to the formation of highly cellular internal macropore structures.

The macropore structure of chars becomes a major factor in determining char reactivity during gasification processes that take place at elevated temperatures and are, therefore, diffusion-limited. Under such conditions, the accessibility of pores to the gaseous reactants has a strong effect on gasification rates. Low utilization of the surface area associated with the micropores is expected and the reactions occur mostly in the larger macropores that are close to the particle exterior. As the reaction proceeds, however, walls of closed pores will burn away exposing surface area previously unavailable for reaction and leading to substantial particle fragmentation. The opening of closed porosity, the formation of a progressively more tortuous particle exterior and the fragmentation of the original particles can lead to large enhancements of the observed gasification rates.

This study presents some of our recent experimental results on the effect of pyrolysis conditions on the macropore structure of coal chars and on their reactivity during combustion with oxygen. The variables we consider are the pyrolysis heating rate, the final heat treatment temperature (HTT), and the soak time at HTT. Pyrolysis and gasification experiments are carried out on (i) a thermogravimetric reactor that provides accurate measurements of volatile evolution and combustion rates and (ii) a microscope hot-stage reactor that allows direct observation of pyrolyzing and burning particles under a microscope. The combination of these two techniques allows us to observe and interpret some interesting transient phenomena such as self-ignition and fragmentation of char particles. Our analysis pays particular attention to combustion at high temperatures where the heterogeneous reactions take place in the regime of strong diffusional limitations.

EXPERIMENTAL PROCEDURES

The coal used was the Illinois #6 from the Argonne premium coal sample collection. Coal particles in the 28-32 mesh (500-595 μm) range were pyrolyzed in a thermogravimetric reactor (Perkin Elmer TGS-2) with a custom-built furnace and computer-controlled heater. For each run, a coal sample of about 1 mg (8-10 particles) was pyrolyzed in nitrogen atmosphere. Pyrolysis experiments were carried out at the following conditions: Heating rates: 0.1, 1 and 10 $^{\circ}\text{C}/\text{s}$; Final heat treatment temperature (HTT): 700, 800 and 900 $^{\circ}\text{C}$; and Soak Time at HTT: 0 and 3 minutes.

The char particles were reacted with oxygen immediately after the pyrolysis stage. The pyrolyzed samples were rapidly cooled from the HTT to 250 $^{\circ}\text{C}$ and a mixture consisting of 20% oxygen and 80% nitrogen was introduced in the reactor. After a few minutes, the samples were rapidly

ramped to the final combustion temperature which varied from 400 °C to 550 °C. The gravimetric capabilities of our reactor allowed us to also obtain a proximate analysis of the volatile and ash content of the coal samples.

A data acquisition and control computer continuously monitored the weight of the samples during both the pyrolysis and combustion stages. The same computer controlled the temperature of the TGA and operated the mass flow controllers that set the gas flow rates. Temperature control was very accurate. During the entire temperature program, the average squared error in temperature was of the order of 1 °C. Raw data (sample weight and temperature vs. time) were stored on a computer disk for later analysis. The weight vs. time data were interpolated with B-splines (using a least squares approximation) and the interpolant was differentiated to obtain the reaction rates.

A microscope hot-stage reactor (Glass and Zygourakis, 1988) was also used for visual observation of the coal particles during the stages of pyrolysis and combustion. The experiments were recorded in video tape and specific images were later digitized on a digital image processor. From the digital images, time resolved measurements of particle swelling were obtained.

RESULTS AND DISCUSSION

Pyrolysis

The experiments on the microscope hot-stage reactor showed that the coal particles swell considerably and that the swelling increases with increasing heating rates. Although we did not characterize in detail the macropore structure of the chars produced during the experiments reported here, our swelling measurements indicate that the char particles have very open cellular macropore structures similar to those quantified via digital image analysis in our earlier studies with the same parent coal (Zygourakis, 1988). As we expected, the heating rate strongly affected the swelling (and therefore the macroporosity) of the char particles.

By continuously monitoring the weight loss of the pyrolyzing coal samples, the instantaneous volatile release rates were obtained and analyzed to elucidate the effects of heating rate. Figure 1a shows the weight loss rates for several runs at two different heating rates. The results for 0.1 and 10 °C/s indicate very good reproducibility and the maximum pyrolysis rate is observed in a rather narrow temperature range for each heating rate. There is, however, a significant shift of this maximum towards higher temperatures as shown in Figures 1a, 1b and Table 1.

Heating rate (°C/s)	0.1	1.0	10
Temperature (°C)	410-425	460-480	510-545

This shifting of the maximum to higher temperatures with increasing heating rates suggests that such experiments can be used to determine the kinetic constants of devolatilization rates. For example, if we assume that the rate of devolatilization can be described by the following simple model

$$\frac{dV}{dt} = k_0 e^{-\frac{E}{RT}} (V^* - V) \quad (1)$$

where $V(t)$ is the fraction of the original coal sample lost up to time due to the release of volatiles and $V(t) \rightarrow V^*$ as $t \rightarrow \infty$ (see Anthony and Howard, 1976). If we set $\theta = (V^* - V) / V^*$, Equation (1) becomes

$$\frac{d\theta}{dt} = -k_0 e^{-\frac{E}{RT}} \theta \quad (2)$$

At the temperature T_m where the maximum devolatilization rate is observed

$$\frac{d^2\theta}{dt^2} = 0 \Rightarrow \exp\left[-\frac{E}{RT_m}\right] = \frac{Eq}{k_0 R T_m^2} \Rightarrow \ln\left(\frac{T_m^2}{q}\right) = \left(\frac{E}{R}\right) \frac{1}{T} + \ln\left(\frac{E}{R k_0}\right)$$

where q is the constant pyrolysis heating rate. The semi-log plot of Figure 2 shows an excellent correlation ($R=0.9998$) and yields $E = 43.4$ kcal/mole and $k_0 = 2.09 \times 10^{11}$. These numbers are in good agreement with other data in the literature. An analysis of these data using a more detailed pyrolysis model is currently under way. Although the weight loss rate changes significantly during the pyrolysis stage, our data show that most of the weight loss occurs during a period when the pyrolysis rate is almost constant. Since the pyrolysis occurs under nonisothermal conditions, this observation agrees with the previous model.

A final observation (Figure 3) is that the amount of released volatiles appears to increase slightly with increasing heating rates. This observation is in agreement with the theoretical predictions (Fletcher et al., 1989) of the chemical percolation devolatilization (CPD) model and the experimental observations of Gibbins-Matham and Kandiyoti (1987). We should note, however, that video microscopic observations of coal particles pyrolyzing at high heating rates show "vigorous bubbling" as volatiles are emitted from the softened coal. This raises the possibility that the escaping volatiles may carry away small fragments of the coal.

Combustion

The combustion rates were computed from the weight vs. time data $m(t)$ according to the formula

$$r(t) = \frac{1}{m(t)} \frac{dm(t)}{dt} \quad (3)$$

where $m(t)$ is the mass of the sample at time t .

Figures 4a and 4b show the evolution of reaction rates with conversion for several char samples prepared at a heating rate of 1 °C/s and three different heat treatment temperatures (HTT): 700, 800 and 900 °C. Soak time at the HTT for all these samples was 3 minutes. The experimental gasification data at 450 °C show the expected char reactivity pattern. Chars produced at a HTT of 700 °C are more reactive than chars produced at higher HTT (800 and 900 °C) and the char reactivity (as measured by $r(t)$) increases continuously with conversion. These observations are in agreement with earlier studies on char combustion (see, for example, Serio et al., 1989) indicating an increase in the molecular order of chars produced at high HTT due to enhanced annealing of the organic and mineral components and the microporosity of the chars. They also agree with theoretical models for gasification in the kinetic control regime where the active surface area associated with the micropores is easily accessible to the reactants (see, for example, Zygorakis and Sandmann, 1988). These and similar models predict that the intrinsic reaction rate will follow an increasing pattern due to the increasing accessibility and specific surface area of the enlarging micropores.

The experimental reactivity curves at 550 °C reveal a different behavior. Figure 4b shows that the reaction rate increases sharply and in a rather "discontinuous" fashion in the early stages of gasification with sharp maxima spanning a conversion range of approximately 10%. After one (or more) such maxima, the reaction rate settles at a fairly constant plateau for the remainder of the reaction. Similar maxima but with smaller amplitude and width can be seen in the reactivity curves of Figure 4a.

We carried out a systematic analysis to make sure that these sharp maxima were not artifacts due to measurement errors or to the interpolation of the numerical data. Figure 5 shows the raw weight and temperature as well as the computed reaction rate for curve A of Figure 4b. By carefully analyzing these and other similar data we concluded that the sudden and sharp drop of the sample weight cannot be due to errors in weight measurements or failures of our controller to maintain constant sample temperature.

We have also carefully analyzed our procedure for obtaining the reaction rates. Usually, our data acquisition system will collect about 300 data points during the pyrolysis stage of each run and 300-3,000 data points during the combustion stage (depending on the reaction temperature). The collected weight vs. time data are interpolated in the least-squares sense (L^2 norm) using B-splines and this polynomial approximation is then differentiated to obtain the observed reaction rate according to Eq. (3). It is essential to determine the appropriate order of polynomials and number of breakpoints to use for the interpolation of the raw weight data. If high order polynomials are used, the reactivity curves will be smoothed out and fine details will be lost. Also, the curves will be very noisy if a large number of breakpoints is used. Our choice of polynomials was dictated by the form of our data that indicated the reaction rate is continuous in time but not necessarily smooth (i.e. it has a discontinuous first derivative). Such behavior has also been observed by Sundback et. al. (1984) who attributed it to particle fragmentation. Our earlier studies (Zygourakis and Sandmann 1988, Zygourakis 1989) indicate that these jumps may also be caused by the opening of large internal pores during combustion in the diffusion-limited regime (high temperatures). Therefore, we decided to use C-1 quadratics for the interpolation instead of the more often used C-2 cubic splines. This assumes that the reaction rate is a linear function of time at each interval and can exhibit sharp maxima and minima which would be smoothed out with a cubic spline. The number of intervals is in most cases larger than 30 and our software allows for dynamic placement of the breakpoints in regions with rapidly changing sample weight, a feature that improves our ability to resolve fine details of the reactivity curve. Since we always have more than 20 data points in each subinterval, any noise disturbances cannot significantly influence our results.

The microscope hot-stage reactor provided the last piece of conclusive evidence that helped us determine the cause of the observed "spikes" in the reactivity curves. Visual observation revealed that some particles ignited, usually during the very early stages of gasification at the higher temperatures (e.g. 550 C). Ignited particles were then rapidly consumed. The width of the spikes corresponds to about 10% total conversion and, thus, spike should be attributable to the ignition of one of the 8-10 particles loaded in our reactor for each run.

All this evidence strongly suggest that the sharp spikes in the reactivity curves are due to **particle ignition**. After the ignited particles are completely consumed, the reaction rate remains almost constant for a wide range of conversion. This behavior is in (at least qualitative) agreement with our gasification models that assume that the macropore structure is the major rate-determining factor in the regime of diffusional limitations (high temperatures). While at first only the outer macropores are available for reaction, closed macropores open up as the reaction front reaches them and the observed reaction rate remains relatively constant.

The jumps observed during reaction in the kinetic control regime may also be caused by a progressive opening of large macropores that makes previously closed micropores accessible to the reactive molecules and creates sharp maxima in the reaction vs. conversion curves. We should also note here that **char particles treated at lower HTT are more likely to ignite at 550 °C.**

Figures 6a and 6b show that longer soaking times at the HTT decrease the reactivity of the char samples. Our results also strongly indicate that the longer soaking time (3 mins) rendered the chars much less likely to ignite at 550 C.

Finally, Figures 7a and 7b provide the strongest evidence of the significant effects of the macropore structure on char reactivity. As we have previously established (Zygorakis, 1988), high pyrolysis heating rates lead to increased particle swelling, large vesicular macropores and higher macropore surface areas. These structural characteristics should lead to (a) more reactive chars when combustion is carried out at high temperatures and (b) reactivity vs. conversion patterns exhibiting sharply increasing rates followed by regions of slowly decreasing or almost constant gasification rates. Figures 7a and 7b clearly show that the chars produced at 1 and 10 C/s are more reactive, exhibit the reactivity patterns that are clearly attributable to their macropore structure and ignite more easily during combustion at 550 °C (Figure 7b). When combustion takes place at 450 °C, the reaction rates do not appear to be significantly influenced by the pyrolysis heating rate and, therefore, by the macropore structure. Still, the reactivity curve for the char produced at a pyrolysis heating rate of 10 °C/s shows some "jumps" whose small amplitude seems to indicate that they are caused by macropore opening (e.g. cenosphere structures) rather than by particle ignition.

CONCLUSIONS

In agreement with literature data, our results show that high heat treatment temperatures and longer soak times result in significant declines in reactivity caused by the increased molecular order of the chars. More importantly, however, the preliminary results presented here clearly indicate that the pyrolysis conditions have strong effects on the macropore structure and, consequently, on the reactivity of the produced chars. They also provide some new insights into the transient phenomena associated with particle ignition and macropore opening during combustion in the diffusion-limited regime of high temperatures.

ACKNOWLEDGMENT

The authors gratefully acknowledge the support for this work provided by the Department of Energy under contract DE-FG22-87PC79930 (James R. Longanbach, Project Manager).

REFERENCES

- Anthony, D.B and Howard, J.B., *AIChE J.*, **22**(4), 625 (1976).
- Fletcher, T.H., Kerstein, A.R., Pugmire, R.J. and Grant, D.M., *ACS Div. of Fuel Chem. Preprints*, **34**(4), 1272 (1989).
- Gibbins-Matham, J. and Kandiyoti, R., *ACS Div. of Fuel Chem. Preprints*, **32**(4), 318 (1989).
- Glass, M.W and Zygorakis, K., *Rev. Sci. Instrum.*, **59**(4), 580 (1988).
- Serio, M.A., Solomon, P.R., Bassilakis, R. and Suuberg, E.M., *ACS Div. of Fuel Chem. Preprints*, **34**(1), 9 (1989).
- Sundback, C.A., Beer, J.M., and Sarofim, A.F., *20th Intern. Symp. on Combustion*, Ann Arbor, MI, p. 1495 (1984).
- Zygorakis, K. and Sandmann, C.W., Jr., *AIChE J.*, **34**(12), 2030 (1988).
- Zygorakis, K., *ACS Div. of Fuel Chem. Preprints*, **33**(4), 1272 (1988).
- Zygorakis, K., *ACS Div. of Fuel Chem. Preprints*, **34**(1), 202 (1989).

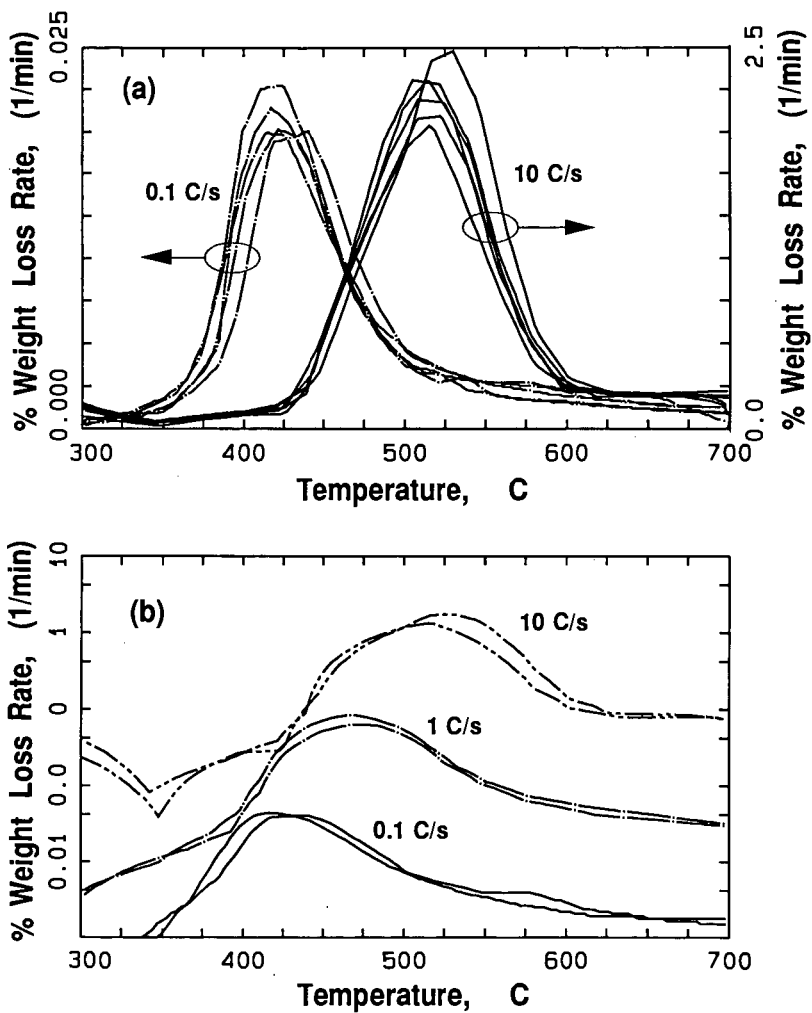


Figure 1: Experimental devolatilization rates for several pyrolysis runs performed at three different heating rates.

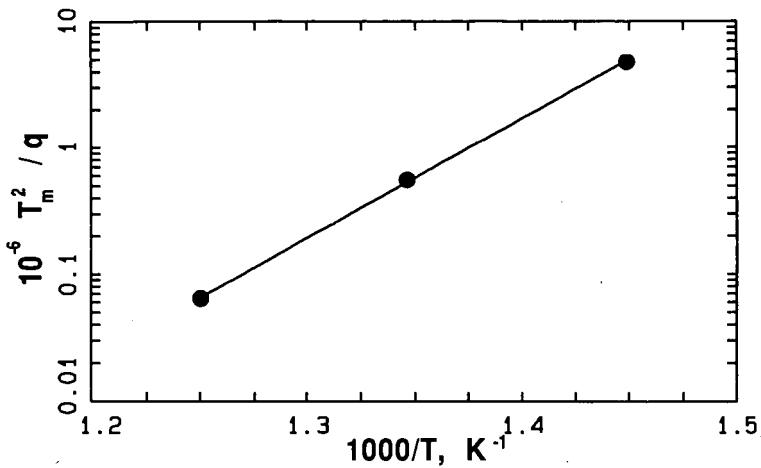


Figure 2: Plot for determining the kinetic constants of the pyrolysis model of Equation (1).

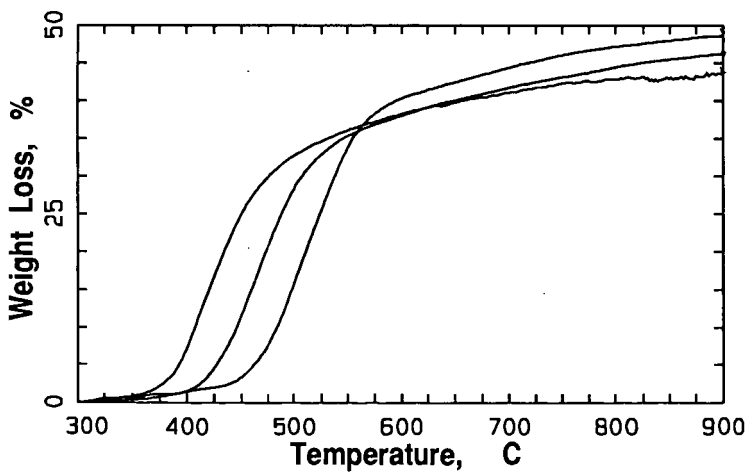


Figure 3: The effect of pyrolysis heating rate on the total amount of released volatiles.

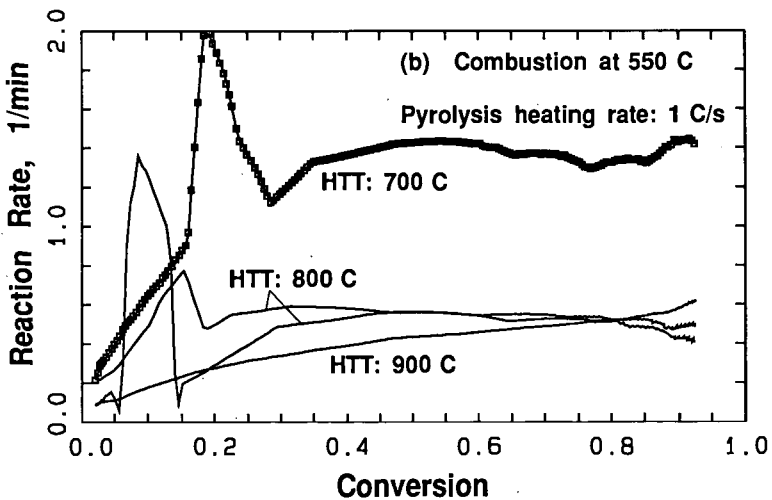
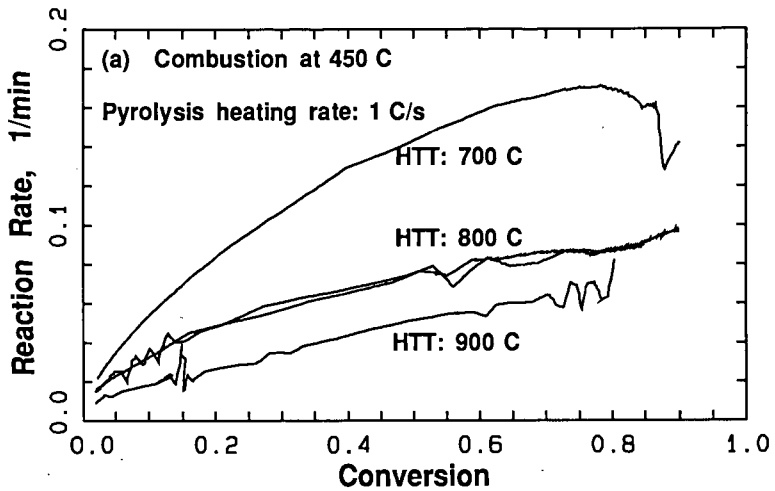


Figure 4: The effect of heat treatment temperature on the reactivity vs. conversion patterns for Illinois #6 chars gasified with oxygen at (a) 450 and (b) 550 °C (Soaking time at HTT: 3 minutes).

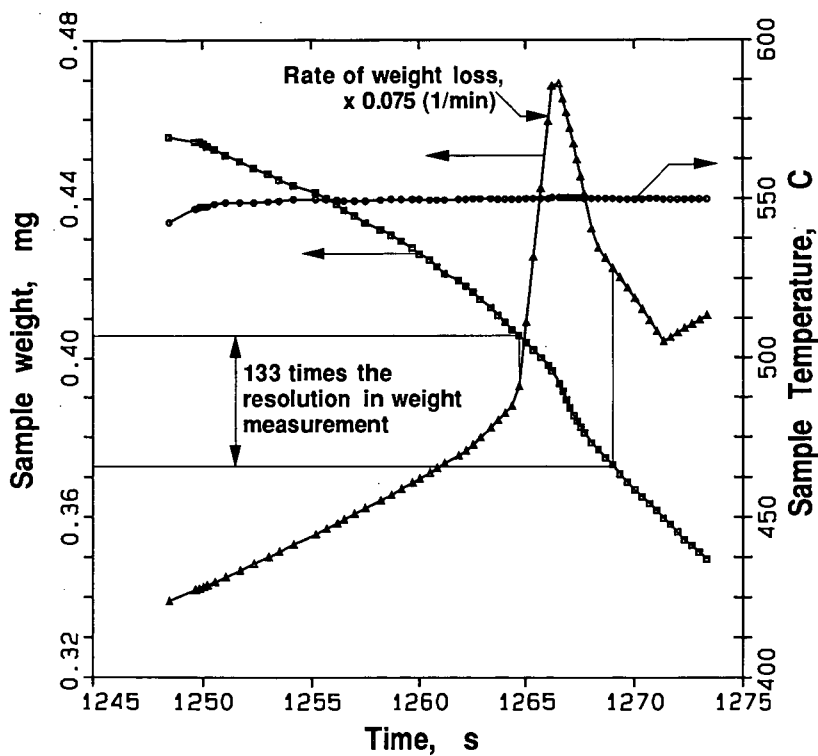


Figure 5: Raw data (sample weight and temperature vs. time) and computed reaction rate for a small part of curve A of Figure 4b.

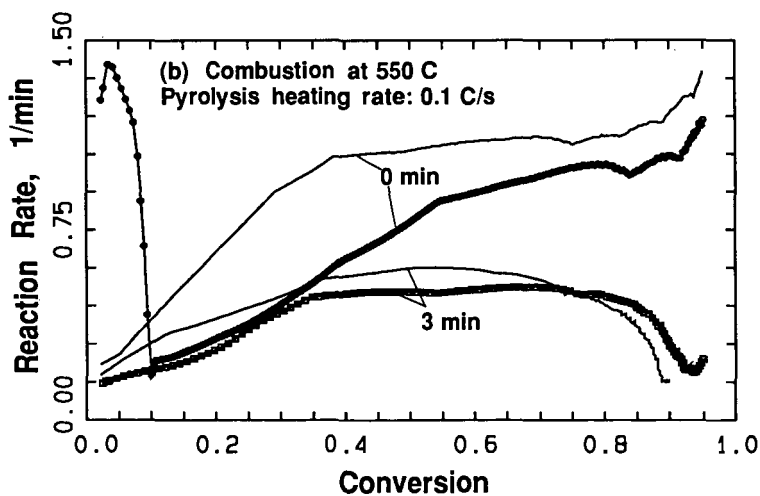
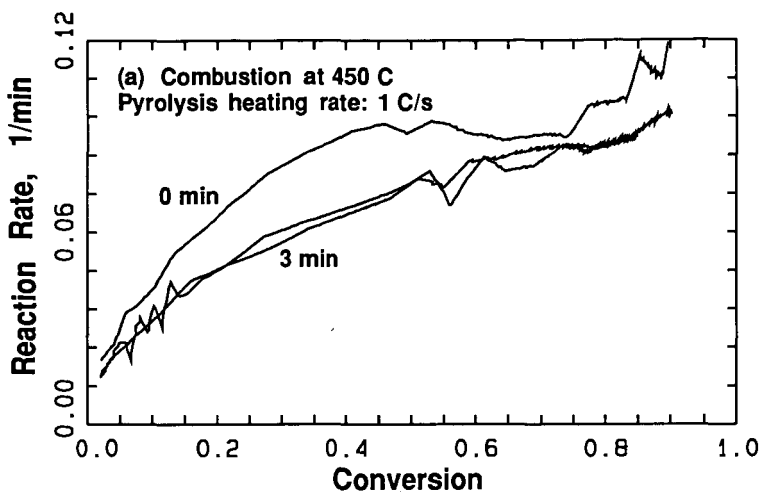


Figure 6: The effect of soaking time on the reactivity vs. conversion patterns for Illinois #6 chars gasified with oxygen at (a) 450 and (b) 550 °C (Heat treatment temperature: 700 °C).

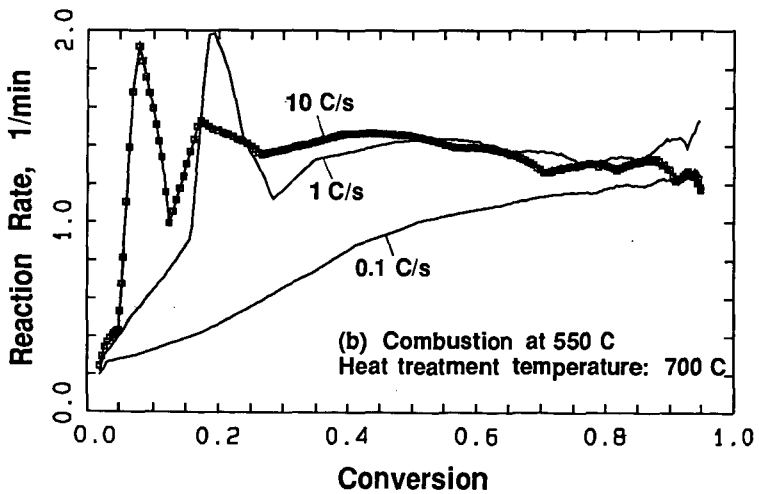
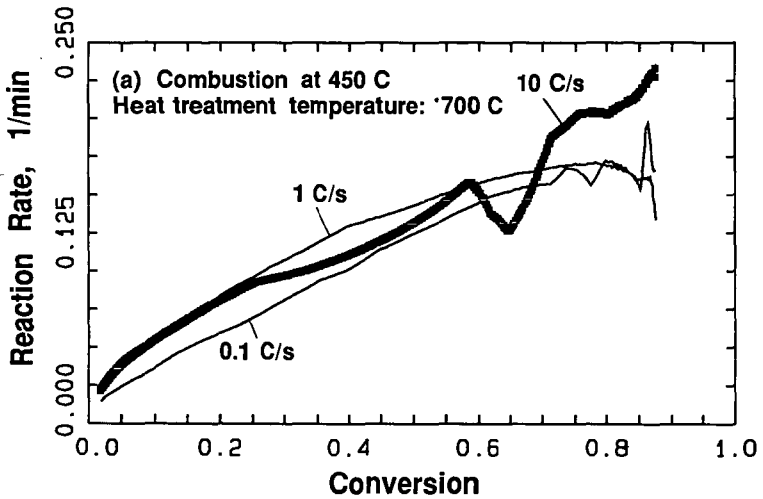


Figure 7: The effect of pyrolysis heating rate on the reactivity vs. conversion patterns for Illinois #6 chars gasified with oxygen at (a) 450 and (b) 550 °C.